Back to Single-carrier for beyond-5G communications above 90 GHz
Grant agreement ANR-17-CE25-0013

D2.1-addendum: Waveform Design for low-power ultra-high data rate systems

---

Authors: Majed Saad and C. Faouzi Bader

CentraleSupélec (*Editor*): Majed Saad and C. Faouzi Bader

October 2021

Contents

1 Introduction **11**

2 Proposed Filter Domain for Index Modulation **13**

3 Proposed SISO FSIM system **17**
3.1 FSIM Transmitter . . . 17
3.2 FSIM Receiver . . . 19
3.2.1 Joint ML Detector . . . 19
3.2.2 Matched Filter-based Detector . . . 20
3.2.3 ISI Estimation and Cancellation . . . 20
3.3 Filter Bank Design requirements . . . 22
3.4 Theoretical Performance Analysis . . . 24
3.5 Numerical Results Analysis and Discussions . . . 26
3.6 FSIM vs Media-Based Modulation . . . 32
3.7 Conclusion . . . 34

4 Proposed MIMO SMX-FSIM system **35**
4.1 Introduction . . . 35
4.2 System Model . . . 36
4.2.1 SMX FSIM Transmitter . . . 36
4.2.2 SMX FSIM Receiver . . . 38
4.3 Theoretical Performance . . . 40
4.4 Results and Discussions . . . 42
4.5 Spectral Efficiency Analysis: SMX-FSIM vs existing MIMO techniques . . . 45
4.6 Conclusion . . . 47

5 Deliverable final conclusions **48**

List of Figures

1 System model of the FSIM-based transmitter and receiver with MF-based detector using N filters of length L and M-ary APM. Note that the MF detector can be replaced by the joint ML detector. . . . 17
2 An example for the Overlap-Add block in the proposed scheme assuming $\eta = 6$ symbols. . . . 18
3 ISI estimation and cancellation using feedback decisions $\{\hat{\imath}, \hat{c}\}$ for past symbols and tentative decisions $\{\tilde{\imath}, \tilde{c}\}$ for future symbols. . . . 21
4 Impulse Response for the two filters used in our simulations compared to RRC pulse-shaping filter, where $\eta = 10$ and $\lambda = 8$. . . . 27
5 Magnitude and phase response of the filter f_1 depicted in Fig. 4. . . . 27
6 Magnitude and phase response of the filter f_2 depicted in Fig. 4. . . . 27
7 Complete responses of the 2 filters obtained after correct matched filtering at the receiver side, where $\eta = 10$ and $\lambda = 8$. . . . 27
8 The error probabilities of filter index detection with ISI estimation and cancellation, perfect ISI cancellation, and the derived theoretical lower bound of 2-FSIM-MQAM ($N = 2$). The SE is: (a) $[3, 4]$ bits/symbol using $M = [4, 8]$, (b) $[5, 6]$ bits/symbol using $M = [16, 32]$. . . . 28
9 Uncoded BER performance of 2-FSIM-MQAM, its analytical lower bound and its equivalent scheme $2M$QAM of the same SE: (a) 3 bits/symbol using $M = 4$, (b) 4 bits/symbol using $M = 8$. . . . 29
10 Uncoded BER performance of 2-FSIM-MQAM, its analytical lower bound and its equivalent scheme $2M$QAM of the same SE: (a) 5 bits/symbol using $M = 16$, (b) 6 and 7 bits/symbol using $M = 32$ and $M = 64$ respectively. . . . 30
11 Spectrum comparison between the proposed FSIM system with 2 non-optimal filters and the conventional transceivers with QAM and RRC filters. . . . 31
12 Complete responses of the 4 filters obtained after correct matched filtering at the receiver side, where $\eta = 10$ and $\lambda = 8$. . . . 31
13 Uncoded BER performance of 4-FSIM-MQAM, its analytical lower bound and its equivalent scheme $4M$QAM of the same SE: (a) 4 bits/symbol using $M = 4$, (b) 6 bits/symbol using $M = 16$. . . . 32
14 Average uncoded BER comparison of different SC schemes with IM in a frequency selective Rayleigh fading: (a) $J = 2$, (b) $J = 4$. . . . 33
15 System model of $N_t \times N_r$ SMX-FSIM transceiver. . . . 37
16 System model of FSIM Modulator with M-ary APM mapping and a filter bank of N filters. . . . 38
17 System model of FSIM demodulator with the controlled-ISI cancellation and detection. . . . 39
18 SER performance of the proposed SMX 2-FSIM-QPSK system and its equivalent SMX-QAM systems of same SE= 12 bpcu and $N_r = 8$. . . . 43
19 SER performance of the proposed SMX 2-FSIM-QPSK system and its equivalent SMX-QAM systems of same SE= 24 bpcu and $N_r = 12$. . . . 44
20 SER performance of the proposed SMX 2-FSIM-QPSK system and its equivalent SMX-QAM systems of same SE= 30 bpcu and $N_r = 16$. . . . 44

21 Maximum SE for different MIMO techniques: $M = 4$ for systems with APM, $N_a = [1, \ldots, N_t - 1]$ for fixed N_a schemes, and $N = 2$ for FSIM. Figure reproduced from [4]. 46
22 Maximum SE for different MIMO techniques: $M = 16$ for systems with APM, $N_a = [1, \ldots, N_t - 1]$ for fixed N_a schemes, and $N = 2$ for FSIM.Figure reproduced from [4]. 47

List of Tables

1 Spectral efficiency of several existing SISO schemes with/without IM. 14
2 Simulation parameters for SISO FSIM and QAM based systems. 28
3 Simulation parameters for MIMO FSIM and QAM based systems. 42
4 Spectral efficiency of different $N_t \times N_r$ MIMO systems. 45
5 Summary of different MIMO techniques for low-power wireless ultra-high data rates systems in sub-THz bands. 48

List of acronyms

ADC Analog-to-digital converter

APM Amplitude-Phase Modulation

AWGN additive white Gaussian noise

BER bit error rate

bpcu bit per channnel use

CCDF Complementary Cumulative Distribution Function

CFO Carrier Frequency Offset

CSI Channel Side Information

DAC Digital-to-analog converter

DCSK differential chaos shift keying

DM Dual Mode

DP Dual-Polarized

DP-GSM Dual Polarized Generalized Spatial Modulation

EE Energy Efficiency

EGSM Enhanced Generalized Spatial Modulation

EIRP Effective Isotropic Radiated Power

ExSSK Extended Space Shift Keying

FD Filter Domain

FDE Frequency Domain Equalization

FDM Frequency Division Multiplexing

FDMA Frequency Division Multiple Access

FSIM Filter Shape Index Modulation

FTN Faster-than-Nyquist

GFDM Generalized Frequency Division Multiplexing

GMM Generalized Multi-Mode

GPPM Generalized Pulse Position Modulation

GSM Generalized Spatial Modulation

HIQ Hybrid In-phase Quadrature

I In-phase

IAI Inter-Antenna Interference

IM Index Modulation

IMMA Index Modulation Multiple Access

IoT Internet of Things

ISI Inter-Symbol Interference

LoS Line-of-Sigh

LPWA Low Power Wide Area

MBM Media-Based Modulation

MC multiple carriers

MF Matched Filter

MIMO Multiple-Input Multiple-Output

ML Maximum Likelihood

MM Multi-Mode

MMSE Minimum Mean-Square Error

NOMA Non-Orthogonal Multiple Access

OFDM Orthogonal Frequency Division Multiplexing

OFDMA Orthogonal Frequency Division Multiple Access

OLA Overlap-Add

OOB Out-Of-Band

OOK On-Off Keying

OSIC Ordered Successive Interference Cancelation

PA Power Amplifier

PAPR peak-to-average power ratio

PDF Probability Density Function

PN Phase Noise

PPM Pulse Position Modulation

PSD Power Spectral Density

PSK Phase-Shift Keying

PWM Pulse Width Modulation

Q Quadrature

QAM Quadrature Amplitude Modulation

QIMMA Quadrature Index Modulation Multiple Access

QSIM Quadrature Subcarrier Index Modulation

RC Reduced Correlation

RF Radio-Frequency

RRC Root-Raised Cosine

SC Single Carrier

SE Spectral Efficiency

SeFDM Spectral-efficient Frequency Division Multiplexing

SER Symbol-Error Rate

SIM Subcarrier Index Modulation

SIMO Single Input Multiple Output

SISO Single-Input Single-Output

SM Spatial Modulation

SMX Spatial Multiplexing

SNM Sub-carrier Number Modulation

SNR signal-to-noise ratio

STFSK Space-Time-Frequency Shift Keying

TA Transmit Antenna

TAC Transmit Antenna combination

THz Terahertz

TIM Time IM domain

VB Virtual Bits

VGSM Variable-N_a GSM

VSIM Variable Subcarrier Index Modulation

WLAN Wireless Local Area Network

ZF Zero Forcing

Executive Summary

In the previous deliverable D2.1 [1], we investigated the spatial Index Modulation (IM) domain and mainly Generalized Spatial Modulation (GSM)-based schemes to achieve low-power ultra-high wireless rates in sub-THz bands. In addition, the GSM Multiple-Input Multiple-Output (MIMO) system performances using spatial IM domain are presented with the achieved link budged, and the proposed Enhanced Generalized Spatial Modulation (EGSM) in high correlated channels is also analyzed. In addition, the study is completed by proposing Dual Polarized Generalized Spatial Modulation (DP-GSM) with its low-complexity detector where an additional layer for indexation is added to enhance the performance and the Spectral Efficiency (SE).

It is worth recalling that the spectral-efficient spatial IM scheme with power-efficient modulation scheme (e.g., GSM-QPSK) is shown to be more advantageous in sub-THz bands than the systems used in recent standards (e.g., IEEE 802.11ax) where Spatial Multiplexing (SMX) with high order Quadrature Amplitude Modulation (QAM) is adopted, this comparison with their optimal detectors is shown in [2]. However, GSM requires a full-RF transmitter architecture (i.e., higher transmitter cost) to maintain its SE while using only few Transmit Antennas (TAs) for multiplexing Amplitude-Phase Modulation (APM) symbols, and it suffers from performance degradation when a Transmit Antenna combination (TAC) index is misdetected due to error propagation to all APM symbols. Consequently, these results and drawbacks motivate us to propose a novel IM domain that provides even higher SE/Energy Efficiency (EE) in Single-Input Single-Output (SISO) prior to its MIMO exploitation. It is worth mentioning that each single bit SE enhancement in the SISO context will be multiplied by the multiplexing order in the MIMO context and leads to important SE gain, especially with larger-scale MIMO. Hence, an intelligent strategy that should significantly impact the overall MIMO system design is to enhance the SE of SISO systems while using power-efficient low-order APMs suitable for sub-THz bands with the current technological limitation and RF impairments. This deliverable D2.1-addendum completes the previously cited work by introducing a novel indexation dimension and a novel modulation scheme in SISO and MIMO.

As a first important achievement in this deliverable, a novel domain for IM, named Filter Domain (FD), is proposed where another degree of freedom for IM is presented. In contrast to existing time, frequency, and spatial IM domains that don't use all the available resources efficiently (e.g., time slots, frequency bands, antennas), the proposed filter IM domain allows to overcome this drawback and reach higher SE and EE gains. Within the filter IM domain/dimension, a novel modulation scheme named Filter Shape Index Modulation (FSIM) is proposed[3]. To the best of our knowledge, this is the first time such an indexing dimension is used as a method for SE and EE enhancement purposes. The pulse-shaping filter is indexed to convey additional information bits to those transmitted in the APM data symbols. The information bits in FSIM are mapped into both signal domain (any M-ary APM) and filter domain. We consider a filter bank with different shapes as a new approach rather than a single pulse shaping filter to further explore the indexation gain. Compared to the joint Maximum Likelihood (ML) detection that considers the joint detection of both filter shape index and APM symbols, we proposed a low-complexity Matched Filter (MF) detector that detects firstly the filter shape being used at the transmitter and then the APM symbols being received. A prominent computational complexity reduction is obtained by MF detector while

reaching the optimal performance.
The proposed scheme demonstrates that Inter-Symbol Interference (ISI) is not necessarily undesirable while it is controllable and predictable since it permits to achieve a higher system capacity compared to systems that enforce zero interference. It is worth mentioning that FSIM maintains its superiority in a frequency selective channel compared to existing QAM or Single Carrier (SC) SISO-IM scheme where FSIM achieves a minimum gain of 4 to 6 dB. Second important achievement is the development of a generalized MIMO SMX system by incorporating FSIM scheme to achieve high SE and EE gain [4]. A simple linear receiver for SMX-FSIM is presented, which is based on Zero Forcing (ZF) sample level equalizer followed by a parallel MF-based detector (any other equalizer can be used if it conserves the indexed information). The proposed parallel detection for SMX-FSIM provides good performance with prominent complexity reduction.
Finally, it is worth mentioning that SMX FSIM has better performance, higher robustness to Phase Noise (PN), lower transceiver cost, higher SE/EE gains, and less power consumption compared to other spectral efficient MIMO candidates. However, these advantages come with a slight receiver complexity increase which is in order of L times higher than other candidates [4], and this complexity can be reduced by proper design of filter bank with a shorter filter of length L while respecting FSIM scheme filter requirements [3], and it will be shown in our future filter bank design publication.
For instance, the proposed SMX FSIM in sub-Terahertz (THz) channel requires much lower signal-to-noise ratio (SNR) (4 -18 dB less than other candidates SMX-QAM and GSM [4]), which is crucial for sub-THz systems with limited output power, and it is the only scheme among the (Dual-Polarized (DP))-GSM and (DP)-SMX-QAM systems that can operate in a medium PN level with linear low complexity receiver. More details about the performance assessment of the proposed uncoded/coded FSIM based system are presented in the deliverable D3.1 [5].

Keywords: Index Modulation (IM), Filter Index Modulation, Filter Domain (FD), Filter Shape Index Modulation (FSIM), pulse-shaping filter, joint maximum likelihood detector, matched filter detector, spectral efficiency, energy efficiency, SISO, MIMO.

1 Introduction

Index Modulation has attracted tremendous attention in the last decade due to its potential enhancement in the system SE and/or EE. In addition, IM is well explored separately and jointly in the spatial, frequency, and temporal domains. The idea of IM is to convey additional information bits implicitly (Virtual Bits (VB)) in the index of the selected element among several possibilities. Note that by using an IM strategy, the receiver should be able to correctly detect the indexed element to deduce the associated VBs. For example, in the spatial IM domain, the indexed element is the antenna while it is the time slot and the frequency band/subcarrier in time IM domain and frequency IM domain, respectively.

In the MIMO context, the different combinations of the indices of transmit or receive antennas are used to convey additional information bits by activating some transmit antennas or targeting some receive antennas. The Spatial Modulation (SM) activates a single antenna at the transmitter side to send an M-ary APM symbol [6]. Consequently, different versions of SM are proposed with a constant or variable number of active antennas to achieve a higher SE gain in [7],[8], and [9].

In the SISO context, the frequency IM domain conveys the VBs by the index of the frequency bands/subcarriers being selected when SC/multiple carriers (MC) waveforms are respectively used, e.g., Orthogonal Frequency Division Multiplexing (OFDM) with Sub-carrier IM (OFDM-SIM) [10]. In addition, the Time IM domain (TIM) counterpart was proposed with SC modulations motivated by their lower peak-to-average power ratio (PAPR) in SC-TIM [13]/SC- Frequency Division Multiple Access (FDMA)-IM (SC-FDMA-IM) [14] where the indexed element is the set of activated time slots/sub-carriers. However, most SISO-IM schemes suffer from low SE gain due to discarding some time/frequency resources.

Furthermore, the time and frequency IM domains are merged with the spatial domain to overcome their limited SE by benefiting from the multiplexing gain as in MIMO OFDM-SIM [15]. A similar combination between these domains may also give a good tradeoff between multiplexing and diversity gains for better performance in a dispersive channel as in Space-Time-Frequency Shift Keying (STFSK) [16].

In brief, the spatial IM domain can enhance the SE/EE and reduce the cost of MIMO systems, depending on the spatial IM scheme being adopted, while the time/frequency IM domain strategies in SISO have a limited SE enhancement and, in some cases, a SE loss but with a better EE for low data rate applications and performance.

In the context of the BRAVE project [17] [18], a higher SE/EE is required to achieve low power ultra-high wireless rates in sub-THz bands that enable many interesting scenarios [19]. In addition, the spatial IM domain considered in [20][21] shows that using IM with power-efficient APM (e.g., Generalized SM-QPSK [22]) is more advantageous than the systems used in recent standards where spatial multiplexing with high order QAM are adopted [2]. Consequently, these results motivate us to propose a novel IM domain that enhances the SE/EE in SISO prior to its MIMO exploitation. It is worth mentioning that each δ bits SE enhancement in SISO context will be multiplied by the multiplexing order in MIMO context. In this technical deliverable, our novel domain for IM is presented where a more significant SE and EE enhancement is targeted in SISO with a better performance compared to the equivalent system with and without IM. Moreover, a novel scheme is proposed to achieve higher SE and EE enhancement. Furthermore, the filter IM domain is incorporated with MIMO SMX to show the different advantages of our proposed domain especially in sub-THz

environment, and it is highlighted that the filter IM domain (e.g. SISO and MIMO based FSIM systems) generalizes many existing IM domains and provides another degree of freedom to better exploit IM advantages. Finally, a conclusion about different MIMO potential candidates is presented and more details about the performance assessment is provided in our deliverable D3.1 [5].

The main contributions of this deliverable are as follows:

1. A novel domain for index modulation, named filter domain (FD), is introduced where another degree of freedom for IM is presented. In addition, the derivatives of this FD and its different potential indexation techniques are discussed.

2. Within the filter domain/dimension, a novel modulation scheme named Filter Shape Index Modulation (FSIM) is proposed. To the best of our knowledge, this is the first time such an indexing dimension is used as a method for SE enhancement purpose. The pulse-shaping filter is indexed to convey additional information bits to those transmitted in the APM data symbols. The information bits in FSIM are mapped into both signal domain (any M-ary APM) and filter domain. We consider a filter bank with different shapes as a new approach rather than a single pulse shaping filter to further explore the indexation gain.

3. The FSIM system model is presented where a low complexity detector based on MF is proposed. Compared to the joint ML detection that considers the joint detection of both filter shape index and APM symbols, the proposed detector performs firstly the filter shape detection and then the APM symbols being received. A prominent computational complexity reduction is obtained.

4. An ISI cancellation is proposed to eliminate the effect of the ISI introduced by the designed filter shapes.

5. Theoretical analysis and Monte Carlo simulations substantiating the efficiency of the proposed FSIM scheme is presented. A lower bound for the error probability of the filter index is derived. In addition, the APM error is incorporated to truly characterize the FSIM system performance in terms of total Symbol-Error Rate (SER) and bit error rate (BER). This lower bound can be evaluated numerically with any number of filters and M-ary APM scheme. Simulation results demonstrate the superior performance of FSIM compared to the other systems of the same SE with/without IM in additive white Gaussian noise (AWGN) and frequency selective fading channels.

6. A simple receiver for SMX-FSIM is presented, which is based on ZF sample level equalizer followed by a parallel MF-based detector. The proposed parallel detection for SMX-FSIM provides good performance with prominent complexity reduction compared to the joint ML-based detector.

7. A generalized MIMO SMX system is proposed by incorporating FSIM scheme to achieve high SE and EE gain. The proposed SMX-FSIM system conveys information bits in the signal and filter IMdomains. The VBs are encapsulated by the different filter shapes indices that are used for pulse shaping of the simultaneously transmitted APM symbols. Note that the transmit spatial IM (e.g., GSM system) conveys all the VBs by a single

index (index of activated TAC), and its misdetection leads to bit errors in most of the VBs and also in the real bits of all transmitted APM symbols (i.e., 0 APM symbols in GSM will be most probably mis-detected when an error occurs in the TAC index detection). However, the decentralization of VBs encapsulation in SMX-FSIM avoids the highlighted single point of failure in GSM system.

8. The analytical performance of SMX-FSIM using ZF equalizer is derived and validated by Monte Carlo simulations. Then, they are compared to those of the conventional SMX QAM system of the same SE. The results show an important SE and EE gain can be achieved even with a low number of filter shapes.

The notations adopted in this Sections 2 and 4 are as follows. Bold lower (upper) case is used for vectors (matrices). The character $*$ denotes the convolution. $(.)^H$, $(.)^T$ and $(.)^{-1}$ are used to denote respectively the Hermitian transpose, the transpose and the inverse of a matrix. $\langle x, y \rangle$ stands for the dot-product. $\mathcal{CN}(\mu, \sigma^2)$ denotes the complex normal distribution of a random variable having mean μ and variance σ^2, $\lfloor x \rfloor$ ($\lceil x \rceil$) denotes the floor (ceil) function that means the largest (smallest) integer less (greater) than or equal to x. The characters $\star$ denotes the cross correlation and f^* denotes the complex conjugate of f. $\|.\|$ stands for the Frobenius norm. The probability of an event is denoted by $P(.)$ and the Probability Density Function (PDF) is denoted by $p(.)$. $\mathbb{E}[.]$ denotes the expectation. C_n^k (n choose k) denotes the binomial coefficient.

2 Proposed Filter Domain for Index Modulation

In general, the time and frequency IM domains have limitations in the SE enhancement for high data rate applications. This limitation is due to the discarding of some available time and frequency resources. The time domain-IM, which activates a time slot to convey information bits, appeared from many decades in several schemes as On-Off Keying (OOK), Pulse Position Modulation (PPM) without APM [23] and Generalized PPM (GPPM) with APM [24]. Then, the SE is enhanced by activating a fixed number of time slots in SC-IM [13], which is proposed with frequency domain equalization (FDE) inspired by the frequency domain counterpart OFDM-Subcarrier Index Modulation (SIM) [10][11]. Similarly, the Generalized FDM-SIM (GFDM-SIM) [12] uses the index of activated frequency bands for the same purpose. Their SE without pulse-shaping rolloff factor effect is expressed in Table 1, where the N time slots or sub-carriers/frequency bands without the cyclic prefix elements of length N_{CP} is divided into G groups of N_g elements ($N = N_g G$), and a fixed N_a ($N_a \leq N_g$) is activated to convey information in IM. The indexation is performed using an acceptable group size N_g to avoid the high detection complexity with a large N. Inspired by OFDM-SIM, the multi-carrier differential chaos shift keying (DCSK) modulation is combined with IM by conveying bits using the activated carrier index and transmitting zero symbols on non-activated ones [25]. Similarly, the IM approach is used with spreading spectrum techniques by selecting one of the predefined spreading codes in Generalized Code Index Modulation [26]. Other IM idea is also investigated in OFDM with Sub-carrier Number Modulation (OFDM-SNM) [27][28], where only the number of activated sub-carriers (N_a value) conveys the VBs. The allowed N_a values for a certain OFDM-SNM system is represented in the set ϕ_g, which can contain

all possible values in the extreme case ($\phi_g = \{1, 2, ..., N_g\}$ where its SE remains lower than conventional M-ary APM).

Table 1: Spectral efficiency of several existing SISO schemes with/without IM.

IM Domain	SC/MC	System Name	Spectral Efficiency	Inherited Interference
-	SC	Linear APM:QAM, PSK,...	$\log_2 M$	No
-	SC/MC	SC-FDE/OFDM	$\frac{N \log_2 M}{N+N_{CP}}$	No
Time	SC	OOK	1	No
Time	SC	PPM [23]	$\frac{\lfloor \log_2 N_g \rfloor}{N_g}$	No
Time	SC	GPPM [24]	$\frac{\lfloor \log_2 N_g \rfloor + \log_2 M}{N_g}$	No
Time	SC	NOMA: IMMA [29]	$\frac{N_u(\lfloor \log_2 N_g \rfloor + \log_2 M)}{N_g}$	YES
Time	SC	NOMA: QIMMA [30]	$\frac{N_u(2\lfloor \log_2 N_g \rfloor + \log_2 M)}{N_g}$	YES
Frequency	SC	NOMA: IM-OFDMA [31]	$\frac{N_u(\log_2 M + \lfloor \log_2 \binom{N_g}{N_a} \rfloor)}{N_g}$	YES
Time Frequency	SC MC	FDE SC-TIM[13], SC-FDMA-IM[14] OFDM-SIM[10][11], GFDM-SIM[12]	$\frac{G(N_a \log_2 M + \lfloor \log_2 \binom{N_g}{N_a} \rfloor)}{N+N_{CP}}$	No
Frequency	MC	OFDM-VSIM [32]	$\frac{G(\lfloor \log_2(\sum_{N_a \in \phi_g} M^{N_a} \binom{N_g}{N_a}) \rfloor)}{N+N_{CP}}$ Extreme case: $\frac{G\lfloor \log_2 (M+1)^{N_g} \rfloor}{N+N_{CP}}$	No
Frequency	MC	OFDM-QSIM [32]	$\frac{G(N_a \log_2 M + 2\lfloor \log_2 \binom{N_g}{N_a} \rfloor)}{N+N_{CP}}$	No
Frequency	MC	OFDM-HIQ-SIM [33]	$\frac{G((N_{a_I}+N_{a_Q}) \log_2 \sqrt{M} + \lfloor \log_2 \binom{N_g}{N_{a_I}} \binom{N_g}{N_{a_Q}} \rfloor)}{N+N_{CP}}$	No
Frequency	MC	OFDM-SNM [27][28]	$\frac{G(N_a \log_2 M + \lfloor \log_2 N_g \rfloor)}{N+N_{CP}}$, $1 \leq N_a \leq N_g$ Average: $\frac{G(0.5(1+N_g) \log_2 M + \lfloor \log_2 N_g \rfloor)}{N+N_{CP}}$	No
Time Frequency	SC SC	FTN-IM [34] SeFDM-IM [35]	$\frac{1}{\nu} \frac{G(N_a \log_2 M + \lfloor \log_2 \binom{N_g}{N_a} \rfloor)}{N+N_{CP}}$	YES
Modulation	SC	DM-FTN-IM [36]	$\frac{1}{\nu} \frac{G(N_a \log_2 M_A + (N_g - N_a) \log_2 M_B + \lfloor \log_2 \binom{N_g}{N_a} \rfloor)}{N+N_{CP}}$	YES
Modulation Modulation	SC MC	DM-SC-IM [37] DM-OFDM-SIM [38]	$\frac{G(N_a \log_2 M_A + (N_g - N_a) \log_2 M_B + \lfloor \log_2 \binom{N_g}{N_a} \rfloor)}{N+N_{CP}}$	No
Modulation	MC	DM-OFDM-VSIM [39]	$\frac{G(\lfloor \log_2(\sum_{N_a \in \phi_g} M_A^{N_a} M_B^{N_g - N_a} \binom{N_g}{N_a}) \rfloor)}{N+N_{CP}}$	No
Modulation	MC	MM-OFDM-IM [40]	$\frac{G(\lfloor \log_2 N_g! \rfloor + N_g \log_2 M)}{N+N_{CP}}$	No
Modulation	MC	MM-OFDM-QIM [40]	$\frac{G(2\lfloor \log_2 N_g! \rfloor + N_g \log_2 M)}{N+N_{CP}}$	No
Modulation	MC	GMM-OFDM-IM [41]	$\frac{G(\lfloor \log_2 N_g! \rfloor + \sum_{k=1}^{K} n_k \log_2 M_k)}{N+N_{CP}}$ where $\sum_{k=1}^{K} n_k = N_g$ and $M_1 > M_2 > ...M_K$	No
Frequency	MC	$\mathcal{L}$-OFDM-SIM [42]	$\frac{G\mathcal{L}(\lfloor \log_2 \binom{N_g - N_a(\mathcal{L}-1)}{N_a} \rfloor + N_a \log_2 M))}{N+N_{CP}}$	No

Moreover, the time and frequency IM domain are adopted with non-orthogonal resources in Faster-Than-Nyquist (FTN-IM) (time domain-IM) and Spectral efficient FDM (SeFDM) (frequency domain-IM), respectively. These systems suffer from inherited interference, but it can compensate some of the SE loss or limited gain of their orthogonal version, depending on the compression factor ν at the price of performance degradation.

Similarly, the IM Multiple access (IMMA) [29] and IM Orthogonal Frequency Division Multiple Access (IM-OFDMA) [31] exploit the appealing advantage of IM in proposing a new Non-Orthogonal Multiple Access (NOMA) in time and frequency, respectively. Note that IMMA is similar to GPPM, whereas it allows resource sharing among N_u users. However, the frequency domain counterpart IM-OFDMA allows to activate N_a subcarriers in contrast to IMMA that uses a single time slot. The SE enhancement of IMMA is doubled

in Quadrature IMMA (QIMMA) [30] by performing separate indexation on the In-phase (I) and Quadrature (Q) components. In other words, QIMMA transmits the real and imaginary parts of the complex symbol through different resources unless the VBs for I and Q are the same. Consequently, these non-orthogonal schemes with a convenient configuration achieve a performance gain that can vanish due to collisions when many users transmit during the same time/frequency resources. Thus, they provide a trade-off between the SE system enhancement and the collision probability that are affected by the maximum number of users in each time/frequency chunk.

Furthermore, several SE enhancements for these SISO-IM are enabled by allowing the activation of a variable number of sub-carriers in OFDM-Variable SIM (OFDM-VSIM) [32] and/or independent sub-carriers activation with the same N_a between the I and Q components in OFDM-Quadrature SIM (OFDM-QSIM) [32] or different N_a between them in OFDM-Hybrid IQ-SIM (OFDM-HIQ-IM)[33]. For the same reason, the Layered-OFDM-SIM ($\mathcal{L}$-OFDM-SIM) is proposed in [42] while taking advantage of modulation type IM domain that uses distinguishable modulations between different layers. In each group of N_g subcarriers, the $\mathcal{L}$-OFDM-SIM scheme activates N_a subcarriers per layer of $N_g - N_a(\mathcal{L}-1)$ elements. This $\mathcal{L}$-OFDM-SIM activates more subcarriers in total ($G\mathcal{L}N_a$) compared to OFDM-SIM ($G\,N_a$), and the former performs another SIM on the remaining non-activated subcarriers successively on the subsequent $\mathcal{L}-1$ layers within each group that help to enhance the SE of OFDM-SIM.

However, the previous techniques do not use all available time/frequency resources that limit the SE enhancement. Hence, a dual-mode (DM) IM is introduced to better compensate for the SE loss or limited gain. Indeed, the non-activated slots/bands are exploited to send different and distinguishable APM symbols by means of modulation type IM, so M_A and M_B-ary APM schemes are used respectively during the primary and secondary activated time slots in DM-SC-IM [37] and DM-FTN-IM [36], and frequency sub-carriers in DM-OFDM-IM as discussed in [38][39]. These DM-IM techniques convey information by the used modulation type, and this idea is extended to Multi-Mode (MM) OFDM-IM (MM-OFDM-IM), where each subcarrier within a group of N_g elements transmits a symbol from different constellation sets, and the permutation of these modulation conveys the VBs, similarly for MM-OFDM-Quadrature IM (MM-OFDM-QIM) but with different indexation on I and Q. Afterward, a Generalized MM-OFDM-IM is proposed in [41] to provide a more flexible choice for SE compared to MM-OFDM-IM, by adjusting the number of subcarriers n_k that use the same modulation order M_k (the special case MM-OFDM-IM is obtained when all M_k are equal to M as shown in Table 1). For more details, the reader is referred to the survey [43] that summarizes most of these IM schemes and those in the spatial IM domain.

It is clear from Table 1 that the SISO-IM schemes that do not fully use the time and frequency resources suffer from SE reduction in most configurations, while the dual and multimode versions that use all resources can achieve limited SE enhancement. Although the SE for single-mode IM schemes is limited, they are promising for low data rate applications, such as the Low Power Wide Area (LPWA) Internet of Things (IoT) devices and machine-to-machine communications, since a better performance can be achieved with some of them compared to conventional APM schemes. In addition, a theoretical EE can be enhanced with low data rate applications to reach 50% for the same SE with $M = 2$ BPSK, $N_g = 4$, $N_a = 2$ as presented in SC-FDMA-IM [14]. However, their EE is dramatically reduced compared to conventional APM schemes (QAM) for high data rate applications. This lower EE is due

to the need for higher power (SNR) to maintain the same SE, by using either higher M-ary APM when not all resources are used according to Table 1, or non-orthogonal schemes with inherited interference.

Aiming at further enhancing the SE gain, the FD is proposed in this section. It will be first applied to SISO systems prior to its exploitation in MIMO context. It is worth mentioning that FD can include all kinds of communication systems because all of these systems have at least one filter used for band-limitation of the signal. In addition, the FD-IM domain allows the indexation of several filter properties to convey information bits with or without an APM symbol. Adopting the FD indexation strategy, one can cover as many schemes as it can be imagined to convey VBs by indexing: the bandwidth, the roll-off factor, the filter shapes, the filter time shift,...etc.

Hence, the frequency IM domain can be seen as a special case of the FD because the activation/deactivation of a frequency band or a subcarrier is just an application of a band-pass/zero filters in single-mode IM. Similarly, the time IM domain counterpart can also be considered as a special case of the FD. Note that in the single-mode time IM domain, the transmitter sends APM symbols only during activated time slots where a non-zero filter is used. In DM-IM, the transmission of data symbols in all time slots or subcarriers is enabled by using distinguishable APM schemes between primary and secondary activated resources. The DM-IM systems in [36]-[38] consider two distinguishable constellation alphabets drawn from the inner and outer constellation points of different average power levels using the same or different normalized constellation points. Note that DM-IM can be achieved by using the same normalized APM alphabets followed by different filters to change power and phase, by using different APM constellations with the same filter or using both different APM constellations and filters between primary and secondary active resources. The filter IM domain generalizes the single-mode IM by selecting only different filters between active and non-active sub-carriers or time slots. However, the filter IM domain also needs to select different APM mapper (constellation alphabets) between the different active resources to generalize all DM-IM and MM-IM cases. Therefore, the filter IM domain can generalize most of SISO IM schemes.
Furthermore, FD-IM also includes the conventional modulation schemes as the Pulse-Position Modulation (PPM), Pulse-Width Modulation (PWM), On-Off Keying (OOK) because they convey bits by means of indexing a filter property. Hence, FD-IM generalizes most of SISO-IM schemes, and its exploration allows more innovation in communication systems.
Many possible indexations in FD (e.g., the filter roll-off) are not explored, currently, because they involve a bandwidth variation, and/or they cannot be modified and detected at the symbol rate, and thus negatively impacting the SE, which is contradictory with our ultimate goal: the SE enhancement. In the following, we will introduce our proposed novel scheme in this IM domain to convey additional information by indexing the filter shapes. This scheme uses all frequency and time resources where the filter shape can be changed at each symbol period to maximize the possible SE enhancement.

3 Proposed SISO FSIM system

3.1 FSIM Transmitter

The proposed system considers a SISO transmission mode, where the binary source information sequence b is divided into two streams b_1 and b_2 as shown in Fig. 1. The bit-stream b_1 is mapped by the M-ary APM, such as QAM or PSK, etc. The bit-stream b_2 is encapsulated in the index i of the selected filter. Then, the selected filter $\mathbf{f}_i[m]$ of length L samples is used as a pulse-shaping filter where m is the sample index taking values between 0 and $L-1$. The filter is truncated in the time domain to η APM symbols and sampled with a rate of λ samples per symbol, which yields $L = \eta.\lambda + 1$ samples. L is restricted to be odd in order to have a linear phase filter without a half sample period shift. We suppose that there is a filter

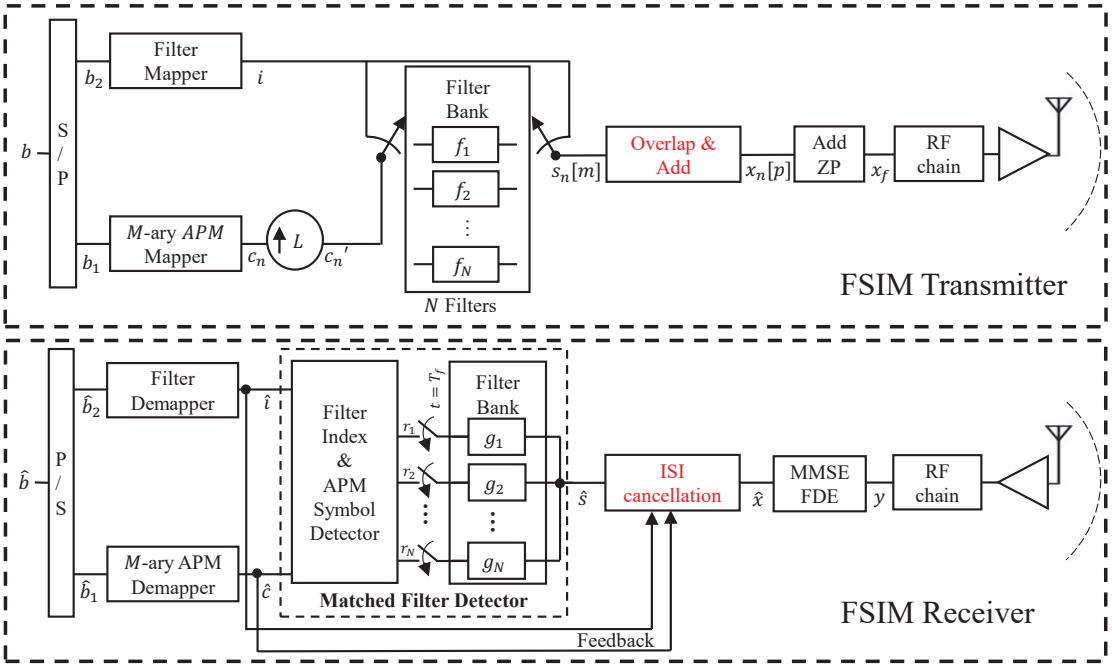

Figure 1: System model of the FSIM-based transmitter and receiver with MF-based detector using N filters of length L and M-ary APM. Note that the MF detector can be replaced by the joint ML detector.

bank with N distinguishable filters as shown in Fig. 1 (N is a power of 2). Accordingly, the number of bits per FSIM symbol $\mathcal{L}_{\text{FSIM}}$ can be expressed as:

$$\mathcal{L}_{\text{FSIM}} = \log_2 N + \log_2 M. \tag{1}$$

Thus, the SE is enhanced by $\log_2 N$ compared to conventional M-ary APM systems thanks to the filter indexation at each symbol period.

The output of the filter bank for the n-th APM complex symbol c_n is denoted by signals $s_n[m]$ and given as follows:

$$s_n[m] = (f_{i_n} * c'_n)[m] = c_n f_{i_n}[m] \tag{2}$$

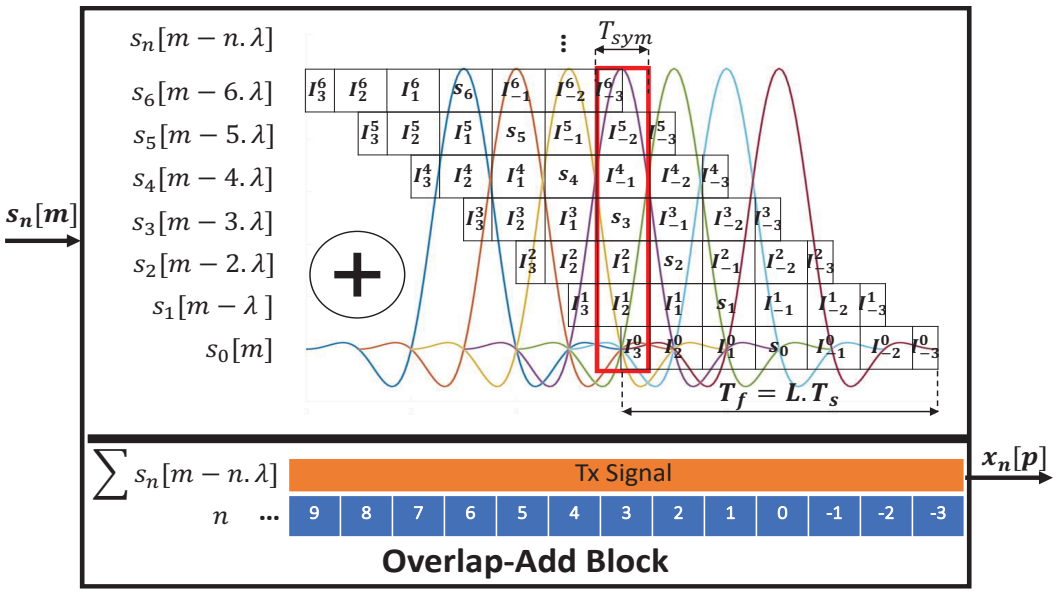

Figure 2: An example for the Overlap-Add block in the proposed scheme assuming $\eta = 6$ symbols.

where c'_n is an up-sampled version of c_n by a factor L, and $i_n \in \{0, 1, ..., N-1\}$ is the index of the filter being selected for the n^{th} symbol according to the bit-stream b_2.

Then, the signals $s_n[m]$ are passed through the Overlap-Add (OLA) block as shown in Fig. 1 in order to generate the λ samples for each APM symbol. The λ desired samples for the n^{th} APM symbol c_n is given by $x_n[p]$ as follows:

$$x_n[p] = \sum_{n'=n-\lceil \eta/2 \rceil}^{n+\lfloor \eta/2 \rfloor} s_{n'}[p - (n'-n)\lambda], \tag{3}$$

where the index $p = p_{\text{center}} - \lceil \lambda/2 \rceil + 1, ..., p_{\text{center}} + \lfloor \lambda/2 \rfloor$ and the index of the middle desired sample is $p_{\text{center}} = \frac{L-1}{2}$.

An example for the OLA with $\eta = 6$ is illustrated in Fig. 2. Note that each row in this figure represents the L output samples of the filter bank for the n^{th} symbol c_n which contains: the desired λ samples $\mathbf{s}_n$ at the center and the undesired samples $\mathbf{I}_j^n$ for $j = \pm 1, \pm 2, \pm 3$. The λ samples $\mathbf{s}_n$ will be affected and interfered by the undesired samples of the $\lceil \eta/2 \rceil = 3$ APM symbols prior the instant n (for $j > 0$) and of $\lfloor \eta/2 \rfloor = 3$ APM symbols posterior to the instant n (for $j < 0$) as depicted in the red vertical box (for $n = 3$) of Fig. 2. Hence, the equation (3) can be rewritten in terms of interference as:

$$\mathbf{x}_n[p] = \mathbf{I}_{\lceil \eta/2 \rceil}^{n-\lceil \eta/2 \rceil} + ... + \mathbf{I}_1^{n-1} + \mathbf{s}_n + \mathbf{I}_{-1}^{n+1} + ... + \mathbf{I}_{-\lfloor \eta/2 \rfloor}^{n+\lfloor \eta/2 \rfloor} \tag{4}$$

Note that the conventional transceiver with any M-ary APM schemes can be considered as a special case from our proposed system where all the filters in the bank are all substituted by the same Nyquist pulse-shaping filter e.g., Root-Raised Cosine (RRC). In other words, the proposed system is equivalent to conventional transceiver when using the same Nyquist filter

for all symbols. Finally, a frame $\mathbf{x}_f$ is created by padding the signal of N_s FSIM symbols by a zero-prefix of length λN_{ZP} samples in order to eliminate the inter-frame interference: $\mathbf{x}_f = [0_1, \ldots, 0_{N_{ZP}}, \mathbf{x}_{-\lfloor \eta/2 \rfloor}, ..., \mathbf{x}_{\lceil N_s - 1 + \eta/2 \rceil}]$. Hence, the SE of FSIM is attenuated by a factor of $N_s/(N_s + N_{ZP})$.

3.2 FSIM Receiver

The receiver scheme proposed by our approach is represented in Fig. 1, where the received signal y is expressed in time domain as:

$$y(t) = (h * x_f)(t) + v(t), \tag{5}$$

where $h(t)$ is the impulse response of a multipath frequency-selective fading channel with J paths and maximum delay spread of $(J-1)T_{sym}$, where $T_{sym} = \lambda.T_s$ is the APM symbol period and T_s is the sampling period. Note that $N_{ZP} \geq (J-1)$ in order to avoid the inter-frame interference. $v(t)$ is the AWGN with zero mean and variance σ_v^2, i.e, $\mathcal{CN}(0, \sigma_v^2)$. The power of transmitted symbols c_n and the used filters f_{i_n} are normalized: $\mathbb{E}[\|c_n\|] = 1$ and $\|\mathbf{f}_i\|^2 = \sum_{m=0}^{L-1} f_i^2[m] = 1$, respectively. Firstly, the receiver compensates for the fading channel distortion on all received samples that contain the implicit information of the selected filter index. For each received frame, the zero-prefix is removed, then a linear equalizer like Minimum Mean-Square Error-FDE (MMSE-FDE) [44] is used to mitigate the channel effect and recover the signal $\hat{x}$ as depicted in Fig. 1.

Afterward, the equalized signal $\hat{x}$ is passed to the ISI estimation and cancellation that remove the controlled ISI from the used filter shapes. The ISI cancellation is required if the used filters don't satisfy the Nyquist ISI criterion. The condition for zero ISI in AWGN channel is:

$$(f_i * g_i)(n.T_{sym}) = \begin{cases} 1 & n = 0 \\ 0 & n \neq 0 \end{cases} \tag{6}$$

for any integer n and $i = 1, ..., N$, where g_i is the impulse response of the MF. Note that when this condition is satisfied, only one pulse has an effect at the integer multiple of the symbol period, as shown in Fig. 2. However, this condition is relaxed in the proposed system when the target is to enhance the SE of M-ary APM, and then ISI will occur naturally. Therefore, an ISI cancellation process is mandatory before detecting the APM symbol and the selected filter index. The APM symbol and index detection can be performed jointly using the joint ML detector or separately using the MF detector. The proposed detectors are described in the following.

3.2.1 Joint ML Detector

The equalized signal $\hat{x}$ is fed to the ISI cancellation block that aims at regenerating free-ISI signals $\hat{\mathbf{s}}$ composed each of L samples. These signals $\hat{\mathbf{s}}$ are then fed to the detector to jointly recover the filter index and the transmitted symbols. The detection can be performed using an ML detector that makes an exhaustive search over all possible APM symbols and filters $\mathbf{f}_i$ combinations as described below:

$$\{\hat{i}, \hat{c}\} = arg \min_{\mathbf{f}_i \in \psi, c \in \chi} \|\hat{\mathbf{s}} - \mathbf{f}_i * c\|^2 \tag{7}$$

where ψ and χ denote the set of N filter's shapes and the M-ary APM constellation, respectively. $\hat{\imath}$ and $\hat{c}$ are the estimated filter index of $\mathbf{f}_i$ and the estimated APM symbol, respectively. Such a receiver's system model is similar to that illustrated in Fig. 1 but by replacing the MF-based detector by an ML detector.

3.2.2 Matched Filter-based Detector

The detection of the selected filter index can be performed using a bank of MFs or a bank of correlators. This subsection will consider the MF-based detector, knowing that both detectors provide the same results [45]. Figure 1 depicts the system model where the detection is performed after the ISI cancellation. The detector is composed of N matched filter g_k where $g_k(t) = f_k(T_f - t)$ with $0 \leq t \leq T_f$, $T_f = L.T_s$. The outputs of these filters $r_k(t)$ are given by:

$$\begin{aligned} r_k(t) &= \int_0^t \hat{s}(\tau) g_k(t-\tau) d\tau, \quad k = 1, 2, \ldots, N \\ &= \int_0^t \hat{s}(\tau) f_k(T_f - t + \tau) d\tau. \end{aligned} \tag{8}$$

These filter outputs are evaluated at the instant T_f

$$r_k = \int_0^{T_f} \hat{s}(\tau) f_k(\tau) d\tau, \quad k = 1, 2, ..., N. \tag{9}$$

Thus, the decision on the selected filter index, being used at the transmitter, is based on selecting the largest energy of the sampled MF outputs as follows:

$$\hat{\imath} = arg \max_k \|r_k\|^2. \tag{10}$$

Once the filter index is detected, $r_{\hat{\imath}}$ is decoded by using the APM detector that determines the ML transmitted symbol $\hat{c}$ in the constellation set χ. Note that any other APM detector can be used. Finally, the detected APM symbol $\hat{c}$ and the filter index $\hat{\imath}$ are sent to the corresponding demappers to deduce the bit-stream $\hat{b}_1$ and $\hat{b}_2$, respectively.

3.2.3 ISI Estimation and Cancellation

The principle of FSIM is to convey additional information bits through the index of the transmission filter being selected at the transmitter. Thus, this modulation's success is based on the capability of detecting correctly at the first stage, the index of the selected filter f_i. For this reason, the filter bank cannot contain only Nyquist filters due to the inherent high cross-correlation between the possible Nyquist filters. One of the solutions that could allow the detection of correlated Nyquist filter is to use the same filter shape for many successive symbols. However, this solution contradicts the FSIM approach, aiming to increase the SE in contrast to other SISO-IM schemes. Therefore, the filter bank used in this modulation is expected to generate ISI but predictable depending on the filter shapes.

Considering an AWGN channel, equation (5) can be rewritten as follows:

$$\begin{aligned} y(t) = x(t) + v(t) &= \sum_n s_n(t - n.T_{sym}) + v(t) \\ &= \sum_n c_n f_{i_n}(t - n.T_{sym}) \ + \ v(t). \end{aligned} \tag{11}$$

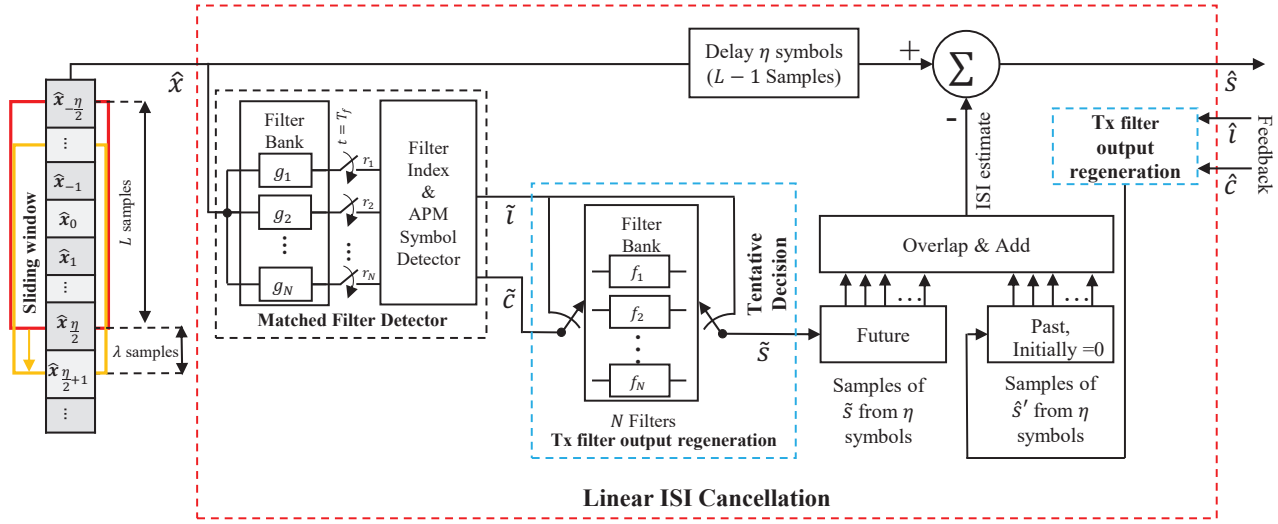

Figure 3: ISI estimation and cancellation using feedback decisions $\{\hat{\imath}, \hat{c}\}$ for past symbols and tentative decisions $\{\tilde{\imath}, \tilde{c}\}$ for future symbols.

The received signal is sampled at the rate of T_s and the L received samples corresponding to APM symbol c_n is given as follows:

$$\begin{aligned} y_n[m] = (&c_n.f_{i_n}[m] \\ &+ \underbrace{\sum_{n'>n} c_{n'}.f_{i_{n'}}[m-(n'-n)\lambda]}_{anticausal \quad ISI} \\ &+ \underbrace{\sum_{n'<n} c_{n'}.f_{i_{n'}}[m-(n'-n)\lambda]}_{causal \quad ISI}) + v_n[m] \\ = &\, c_n.f_{i_n}[m] + ISI_n[m] + v_n[m], \end{aligned} \tag{12}$$

where f_{i_n} represents the i^{th} filter used to transmit the n^{th} symbol and $v_n[m]$ is the noise sampled at $t = n.T_{sym} + m.T_s$. Note that if the used pulse-shaping filters satisfy Nyquist condition for zero-ISI, then the received signal in AWGN channel is ISI free ($ISI = 0$ in (12)) which is not the case in the proposed system.

Thus, the perfect ISI cancellation for the L samples around any symbol requires the knowledge of the filter index and APM symbols for the η past and η future symbols (as shown in Fig. 2 where the ISI in the samples $\mathbf{l}_3^0$ of the first APM symbol c_0 can be eliminated by knowing all the future $\eta = 6$ symbols). The proposed ISI cancellation algorithm takes the past η detected APM symbols $\hat{c}_{n'<n}$ along with their filter indices $\hat{\imath}_{n'<n}$ as a feedback from the previous final decisions as shown in Fig. 1. However, a tentative decision as in [46] is required for the η future symbols. Thus, the ISI cancellation and detection for the current symbol will be delayed by η symbols after receiving the L samples of c_n as depicted in Fig. 3 in order to be able to mitigate the anticausal ISI. Note that the conventional transceiver delay is $d_{\text{conv.}} = \frac{\eta.\lambda}{2} + \lfloor \frac{\lambda}{2} \rfloor$ samples, which corresponds to filter ramp-up delay and time needed to receive all λ samples for first symbol. Thus, the additional FSIM system delay compared to conventional transceiver is $d_{\text{FSIM}} = L + \eta\lambda - d_{\text{conv.}} = 3\frac{\eta.\lambda}{2} + 1 - \lfloor \frac{\lambda}{2} \rfloor$ samples, which cor-

responds to the delay needed to receive the rest of the first L samples and to eliminate the anticausal ISI from the η future symbols.

The FSIM receiver with linear ISI cancellation is depicted in Fig. 3. The tentative decision of the APM symbol $\tilde{c}_{n'>n}$ and the filter index $\tilde{\imath}_{n'>n}$ for future η symbols are detected by the matched filter as described in the subsection 3.2.2 using their corresponding L samples of the received signal $y_{n'}[m]$. These tentative decisions $\{\tilde{\imath}_{n'}, \tilde{c}_{n'}\}$ are used to regenerate the filter bank output originally generated at the transmitter side as $\tilde{s}_{n'}[m] = \tilde{c}_{n'} f_{\tilde{\imath}_{n'}}[m]$. Similarly, this regeneration is performed for the past symbols using the feedback decisions $\{\hat{\imath}_{n'}, \hat{c}_{n'}\}$ to get $\hat{s}_{n'}[m] = \hat{c}_{n'} f_{\hat{\imath}_{n'}}[m]$. As shown in Fig. 3, the regenerated signals are saved in their corresponding registers and then used to generate the ISI estimation. Finally, the ISI cancellation is performed by subtracting the estimated ISI from the corresponding L samples of the received signal $y_{n'}[m]$. This aims to generate the estimated transmitter filter output $\hat{s}_n[m]$ for the APM symbol c_n that can be expressed as follows:

$$\hat{s}_n[m] = c_n f_{i_n}[m] + ISI_{resid}[m] + v_n[m], \tag{13}$$

where $m = 0, ...L-1$. The $ISI_{resid}[m]$ represents the residual ISI that might still persist due to the non-perfect ISI cancellation. Note that if the filters are well designed, the $ISI_{resid}[m]$ approaches zero. Finally, $\hat{s}_n[m]$ is passed through the filter index and the APM symbol detectors to recover the bitstreams b_1 and b_2 as described in Fig. 1.

3.3 Filter Bank Design requirements

Note that the proper design of the filter shape is crucial to allow the correct detection of the indexed filter. In this section, the filter bank design problem is presented, which is similar to the conventional pulse-shaping problem, but more constraints are added to maximize the correct detection of the selected filter index. The proposed system insists that ISI is not necessarily undesirable while it is controllable. The aim is to achieve better system capacity rather than enforcing zero interference.

The filter bank design problem is not a trivial task because all filters f_i in the bank should be jointly designed to satisfy the following conditions and constraints:

1. f_i is strictly band-limited with a bandwidth B within the channel bandwidth B_c, where $B \leq B_c$ should be as large as possible. In addition, the filters f_i should be around the center frequency of the channel (around the carrier frequency in the pass-band or around zero in the base-band).

2. All the filters should have an acceptable level of Out-Of-Band (OOB) radiations with a feasible filter length. Thus, the Magnitude response $|F_i(\omega)|$ of all filters $\mathbf{f}_i$ should satisfy the following condition: $|F_i(\omega)| \leq OOB_{max}$ for $\omega \geq \omega_s$, where ω_s is the stop-band angular frequency. The bandwidth and OOB requirements can be expressed together by set of constraints to fit within a spectral mask.

3. Minimum cross-correlation between all normalized filters f_i in the bank is required to maximize the correct filter index detection at the receiver side. The cross-correlation

between two filters f_i and f_j from the bank is given by:

$$(f_i^* \star f_j)[d] = \sum_{l=-\infty}^{l=+\infty} f_i^*[l].f_j[l-d], \quad \forall\, i,j = 1,2,...,N \text{ and } d = 0,2,...,2L-1. \tag{14}$$

More precisely, the dot-product square between filters $\langle \mathbf{f}_i, \mathbf{f}_j \rangle^2$ should be minimized since the MF detector output taken at $t = T_f$ depends on this dot-product value.

4. The performance of FSIM depends on the ability of correct ISI estimation and cancellation and mainly on the correct tentative decisions in the presence of ISI. Thus, the introduced ISI distortion should be minimized while respecting the previous conditions and constraints, to avoid any error floor in terms of SER and BER.

5. The filter length L should be kept the minimum possible to allow practical implementation. Hence, the tails of their impulse responses should decay to zero after a feasible number of symbols in order to have, after the time domain truncation to η symbols, the best trade-off filter length-OOB.

A straightforward solution for this filter design problem is to have orthogonal filters that occupy each different bandwidth by dividing B_c into N sub-bands. In this case, the first condition to have the same center frequency is not satisfied, which will lead to a lower SE when high M-ary schemes are used according to Table 1. This filter design case leads to a system like in [10] when applying IM in the frequency domain on the OFDM sub-carriers. Hence, the frequency IM domain is a special case of the proposed filter index modulation without a noticeable SE enhancement.
Finally, for a proper filter shape design, we have to minimize the injected ISI distortion from all filters (denoted by ISI_{metric}), while keeping the cross-correlation between all filter-shapes below a threshold ϵ and respecting a predefined spectral mask. Thus, this challenging filter bank design can be formulated as an optimization problem for a given filter length L as follows:

$$\begin{aligned}
\mathbf{P1}: \quad & \underset{\mathbf{f}_1,\ldots,\mathbf{f}_N}{\text{minimize}} \quad ISI_{metric} && \text{(15a)}\\
& \text{subject to} \\
& |F_i(\omega)| \text{ within a predefined spectral mask} && \text{(15b)}\\
& \qquad \forall\, i \in \{1,\ldots,N\}, \\
& \langle \mathbf{f}_i, \mathbf{f}_j \rangle^2 \leq \epsilon && \text{(15c)}\\
& \qquad i \neq j, \forall\, i \text{ and } \forall j \in \{1,\ldots,N\}, \\
& \|\mathbf{f}_i\|^2 = 1 && \text{(15d)}\\
& \qquad \forall\, i \in \{1,\ldots,N\}.
\end{aligned}$$

Such a problem is not tackled previously in the literature where N filter shapes are to be designed jointly with similar constraints. This problem will be properly addressed and discussed in our future publication due to the page limitation.

3.4 Theoretical Performance Analysis

In this sub-section, the probability of error for the filter index is evaluated, then the SER and the total BER is deduced to truly characterize the FSIM system performance in AWGN channel. Note that both proposed detectors (MF and joint ML) achieve similar performance (negligible difference), as it will be shown in the next section. For this reason, the low complexity MF-based detector is only considered in the following theoretical derivations.

The probability of error for filter index pilots the system performance because the error in filter detection leads to an additional ISI, and thus more errors can appear in the detection of APM symbols.

For each symbol period, the input to matched filter detector is the L samples as expressed in (13). In the following, we will assume that the filter bank is well designed where the ISI is perfectly canceled (*i.e.*, $ISI_{resid} = 0$). Hence, the probability of error that will be derived can be considered as the lower bound of the proposed system.
The output of the matched filter bank sampled at $t = T_f$ given by r_k in (9) can be rewritten as:

$$\begin{aligned} r_k &= \langle \mathbf{f}_k, \mathbf{f}_{i_n} \rangle . c_n + \langle \mathbf{f}_k, \mathbf{v}_n \rangle \\ &= \begin{cases} c_n + \langle \mathbf{f}_k, \mathbf{v}_n \rangle & \text{for } k = i_n \\ \langle \mathbf{f}_k, \mathbf{f}_{i_n} \rangle . c_n + \langle \mathbf{f}_k, \mathbf{v}_n \rangle & \text{for } k \neq i_n \end{cases} \end{aligned} \tag{16}$$

Note that when the N filters are orthogonal $\langle \mathbf{f}_k, \mathbf{f}_i \rangle = 0$, the system will be transformed into frequency band indexation, which results in a limited SE enhancement. However, in our proposed system, the filters are not orthogonal because they occupy the same bandwidth, and they have the same center frequency to target a more significant SE enhancement.

To evaluate the probability of error, let us suppose that the filter f_1 is selected at the transmitter side for the APM symbol c_n. Then, the vector $\mathbf{r}_k$ composed of the elements r_k for $k = 1, ..., N$ is given as follows:

$$\mathbf{r}_k = [c_n + v_1, \langle \mathbf{f}_2, \mathbf{f}_1 \rangle . c_n + v_2, ..., \langle \mathbf{f}_N, \mathbf{f}_1 \rangle . c_n + v_N], \tag{17}$$

where $v_k = \langle \mathbf{f}_k, \mathbf{v}_n \rangle$ are complex valued zero-mean mutually statistically independent Gaussian random variables with equal variance $\sigma^2 = \sigma_k^2 = \frac{1}{2} N_0$, where N_0 is the noise spectral density [45]. According to (10), the detection of the filter index selects the maximum $U_k = \|r_k\|^2$ which represents the energy of r_k. U_k is described as a statistically independent non-central chi-square distribution [45] for all k, each having 2 degrees of freedom where the non-centrality parameter α^2 with the energy of APM symbol $\mathcal{E}_q$ is given by:

$$\alpha_{k,q}^2 = \begin{cases} \|c_n\|^2 = \mathcal{E}_q & for\, k = 1 \\ \langle \mathbf{f}_k, \mathbf{f}_1 \rangle^2 . \|c_n\|^2 = \langle \mathbf{f}_k, \mathbf{f}_1 \rangle^2 . \mathcal{E}_q & for\, k \neq 1, \end{cases} \tag{18}$$

where $\mathcal{E}_q$ is the energy of the transmitted APM symbol c_n. Thus, we obtain the PDF of U_k as

$$p(u_k) = \frac{1}{2\sigma^2} e^{-\frac{u_k + \alpha_k^2}{2\sigma^2}} \mathcal{I}_0 \left(\frac{\alpha_k \sqrt{u_k}}{\sigma^2} \right), \tag{19}$$

where $u_k \geq 0$ and $\mathcal{I}_0(\rho)$ is the zero order modified Bessel function of 1^{st} kind given by [45]:

$$\mathcal{I}_0(\rho) = \sum_{\beta=0}^{\infty} \frac{(\rho/2)^{2\beta}}{(\beta!)^2} \quad \rho \geq 0. \tag{20}$$

The error probability of the filter index can be deduced by deriving the probability that the detector makes a correct index decision. This is the probability that u_1 is larger than all other $N-1$ u_k values for $k \neq 1$. This probability of correct decision for a given APM symbol energy $\mathcal{E}_q$ may be expressed as:

$$\begin{aligned} P_{c,\mathcal{E}_q} &= P(U_2 < U_1, U_3 < U_1, ..., U_N < U_1) \\ &= \int_0^\infty P(U_2 < U_1, ..., U_N < U_1 | u_1).p(u_1)du_1 \end{aligned} \tag{21}$$

where $P(U_2 < U_1, U_3 < U_1, ..., U_N < U_1|U_1)$ denotes the joint probability that $u_2, u_3, ...u_N$ are all less than u_1 conditioned on a given u_1. Then, this joint probability is averaged over all u_1. The filters are considered orthogonal when deriving the lower bound, thus these $N-1$ variables u_k becomes statistically independent under this assumption with chi-square distribution ($\alpha^2_{k,q} = 0$ for $k \neq 1$). Since the u_k are statistically independent, the joint probability can be factorized as a product of $N-1$ marginal probabilities of the form:

$$P(u_k < u_1|u_1) = \int_0^{u_1} p_{u_k}(x_k)dx_k, \quad k = 2, 3, ..., N. \tag{22}$$

Thus, the probability of a correct decision is given by:

$$\begin{aligned} P_{c,\mathcal{E}_q} &= P(U_2 < U_1, U_3 < U_1, ..., U_N < U_1) \\ &= \int_0^\infty \left(\prod_2^N P(u_k < u_1|u_1) \right) .p(u_1)du_1, \end{aligned} \tag{23}$$

and the probability of a filter index error with a given APM symbol energy $\mathcal{E}_q$ is as follows:

$$P_{e,\mathcal{E}_q} = 1 - P_{c,\mathcal{E}_q}. \tag{24}$$

Hence, the average probability of filter index error is the weighted average of filter error over the Q possible energy levels of APM symbols, given as follows:

$$P_{e,filter} = \sum_{q=1}^{Q} P_{e,\mathcal{E}_q}.P(\mathcal{E}_q), \tag{25}$$

where $P(\mathcal{E}_q)$ is the probability of occurrence of the energy level $\mathcal{E}_q$. For example, when the used APM is 16-QAM, there are $Q = 3$ possible energy levels $\mathcal{E}_q = [0.2, 1, 1.8]$ and their probability of occurrence is $P(\mathcal{E}_q) = [0.25, 0.5, 0.25]$ if all APM symbols are equiprobable.
An erroneous detection of a filter index leads to the attempt of APM demodulation using the signal output of an mismatched filter with more ISI most probably. Thus, the total probability of APM symbol error $P_{e,APM}$ in FSIM system can be written according to the law of total probability as follows:

$$\begin{aligned} P_{e,APM} &= P_{(APM\,error \cap correct\,filter)} \\ &\quad + P_{(APM\,error \cap false\,filter)} \\ &= (1 - P_{e,filter}) P_{(APM\,error/correct\,filter)} \\ &\quad + P_{e,filter} P_{(APM\,error/false\,filter)}, \end{aligned} \tag{26}$$

where $P_{APM\,error/correct\,filter}$ ($P_{APM\,error/false\,filter}$) is the probability of APM symbol error knowing that the filter index is correctly estimated (mis-detected). Hence, we are deriving the lower bound under the perfect ISI cancellation assumption, then the probabilities of APM symbol error in both cases are equal to the probability of APM symbol error in conventional transceiver with Nyquist filters while using the signal to noise and interference ratio (SNIR) instead of SNR. The calculation with SNIR is required when computing ($P_{APM\,error/false\,filter}$) to consider the known interference resulting from the mismatched filter shapes that exists even in case of perfect ISI cancellation of the past and future symbols.

Consequently, the correct FSIM symbol detection occurs when both the filter and the APM symbol are correctly estimated, then the probability of a correct FSIM decision is $(1 - P_{e,filter})(1 - P_{e,APM})$ and the SER is given by:

$$SER = 1 - (1 - P_{e,filter})(1 - P_{e,APM}). \tag{27}$$

The average probability of virtual (real) bit error can be deduced from filter (APM symbol) error similar to [45, p. 262 (5-2-24)], thus they can be expressed respectively as follows:

$$P_{b,filter} = \frac{N}{2(N-1)} P_{e,filter} \tag{28}$$

$$P_{b,APM} = \frac{M}{2(M-1)} P_{e,APM}, \tag{29}$$

Similarly to SER, the total BER is deduced but while taking into consideration the weight of real and virtual bits:

$$BER = \frac{\log_2 N}{\mathcal{L}_{\text{FSIM}}} P_{b,filter} + \frac{\log_2 M}{\mathcal{L}_{\text{FSIM}}} P_{b,APM}. \tag{30}$$

Finally, we should mention that the cross-correlation between all filters affects the proposed system's performance and should be minimized to enhance the system performance. Besides, the introduced ISI by all filters should also be minimized to approach the lower bound of the error probability for the filter index that affects the APM symbols' detection. This probability confirms that the proposed system's success is based on the filter bank design where the cross-correlation of these filters and their introduced ISI should be jointly minimized. Finally, these theoretical lower bound for error probabilities of filter index detection and BER are validated in the next section.

3.5 Numerical Results Analysis and Discussions

In this section, firstly, the theoretical error probability of filter index detection (25) using the MF-based detector is evaluated and compared to the numerical results obtained with Monte Carlo simulations under different configurations. Secondly, the performance of the proposed system is evaluated when a joint ML and an MF-based detector are employed and compared at different transmission rates to the theoretical lower bound (30) and to the performance of the equivalent APM scheme of the same SE in AWGN channel and a multipath frequency-selective fading channel.

It is worth mentioning that the filter bank design of N filter shapes is not a trivial problem with these new constraints and conditions. For this reason, we designed 2 and 4 non-optimal

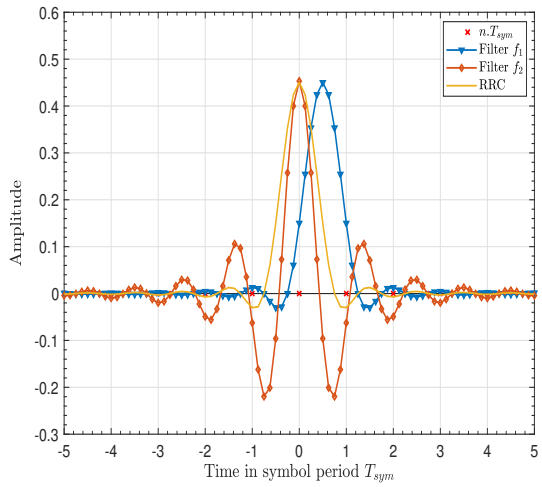

Figure 4: Impulse Response for the two filters used in our simulations compared to RRC pulse-shaping filter, where $\eta = 10$ and $\lambda = 8$.

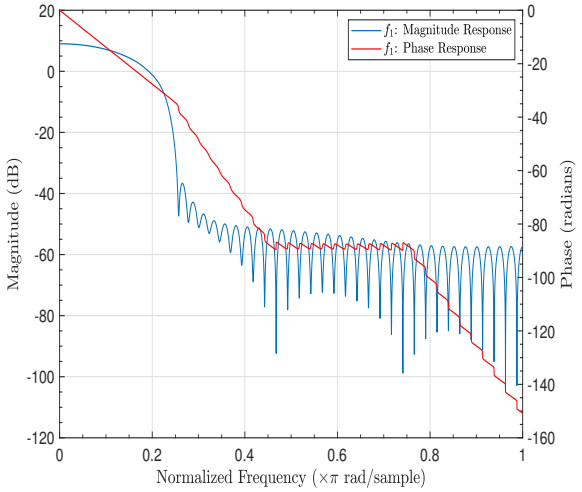

Figure 5: Magnitude and phase response of the filter f_1 depicted in Fig. 4.

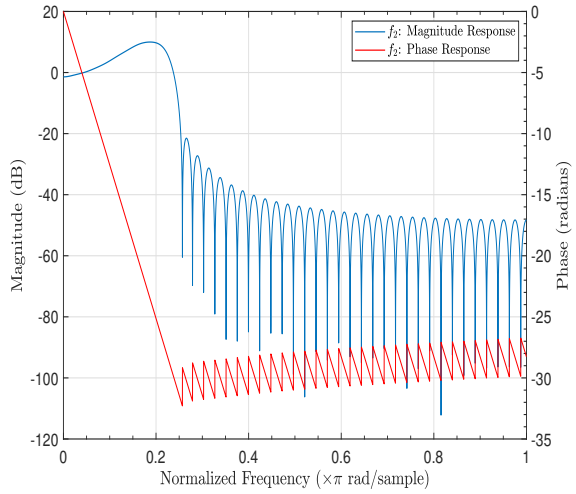

Figure 6: Magnitude and phase response of the filter f_2 depicted in Fig. 4.

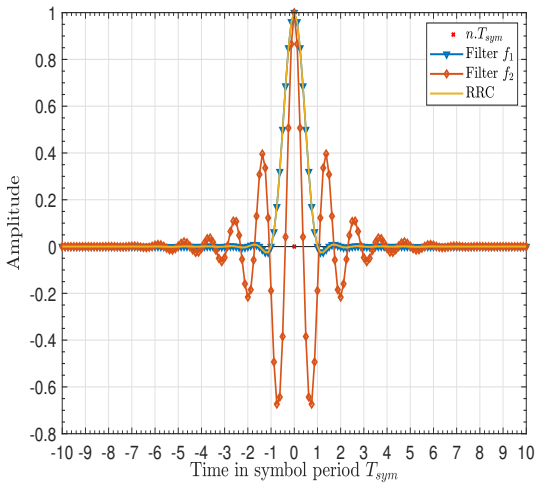

Figure 7: Complete responses of the 2 filters obtained after correct matched filtering at the receiver side, where $\eta = 10$ and $\lambda = 8$.

filter shapes to prove the feasibility of the proposed scheme and to illustrate the minimum performance gain and SE enhancement that can be achieved. The impulse responses of the two filters are presented in Fig. 4, and their magnitude and phase responses are shown in Fig. 5 and 6. Note that the dot product of these filters is $\langle \mathbf{f}_1, \mathbf{f}_2 \rangle = 0.2057$. Moreover, the complete filter responses at the receiver, after correct matched filtering $(\mathbf{f}_i * \mathbf{g}_i)$ are depicted in Fig. 7. The introduced ISI clearly appears in f_2 because the result of $\mathbf{f}_2 * \mathbf{g}_2$ doesn't have a zero-crossing at $t = n.T_{sym}$ for all n.

The proposed system is studied at different transmission rates (3 to 7 bits/symbol) by using different numbers of filter shapes and different QAM orders. The used simulation

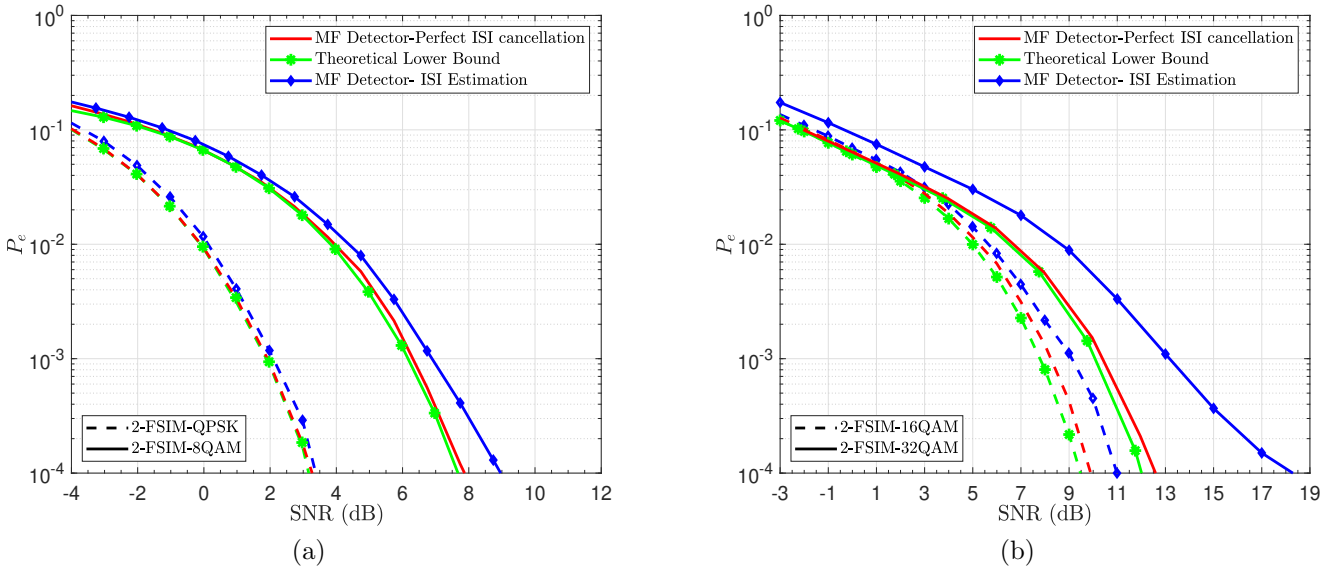

Figure 8: The error probabilities of filter index detection with ISI estimation and cancellation, perfect ISI cancellation, and the derived theoretical lower bound of 2-FSIM-MQAM ($N = 2$). The SE is: (a) $[3, 4]$ bits/symbol using $M = [4, 8]$, (b) $[5, 6]$ bits/symbol using $M = [16, 32]$.

parameters are summarized in Table 2.

Table 2: Simulation parameters for SISO FSIM and QAM based systems.

Parameters	Value
M-ary QAM	$[4, 8, 16, 32, 64]$
N	$[2, 4]$
η	10
Oversampling factor: λ	8
Number of symbols	5×10^5
Pulse-shaping filter for Conventional Transceiver	Root Raised Cosine (RRC)

Figures 8a and 8b compare the theoretical lower bound (25) and simulated probabilities of error of filter index detection with perfect ISI cancellation, and with ISI estimation and cancellation as described in subsection 3.2.3. Note that perfect ISI cancellation means that the tentative decisions for filter index and APM symbol are correctly detected, but those decisions for past symbols are fed back after the final detection. This comparison is performed with $N = 2$ filters and different M-ary QAM where the notation $N-$FSIM$-M$APM is adopted for our proposed system's performance analysis.

It can be observed from Figs 8a-8b that the theoretical lower bound (25) derived under the assumption of perfect ISI cancellation and orthogonal filters matches the simulation results of perfect ISI cancellation with a small difference due to non-orthogonal filters (dot-product is 0.2057), and thus the theoretical lower bound is validated. In addition, the performance of 2-FSIM-QPSK with ISI estimation is near the optimal ISI cancellation as shown in Fig. 8a, because QPSK can support a high ISI level without leading to a false detection (high

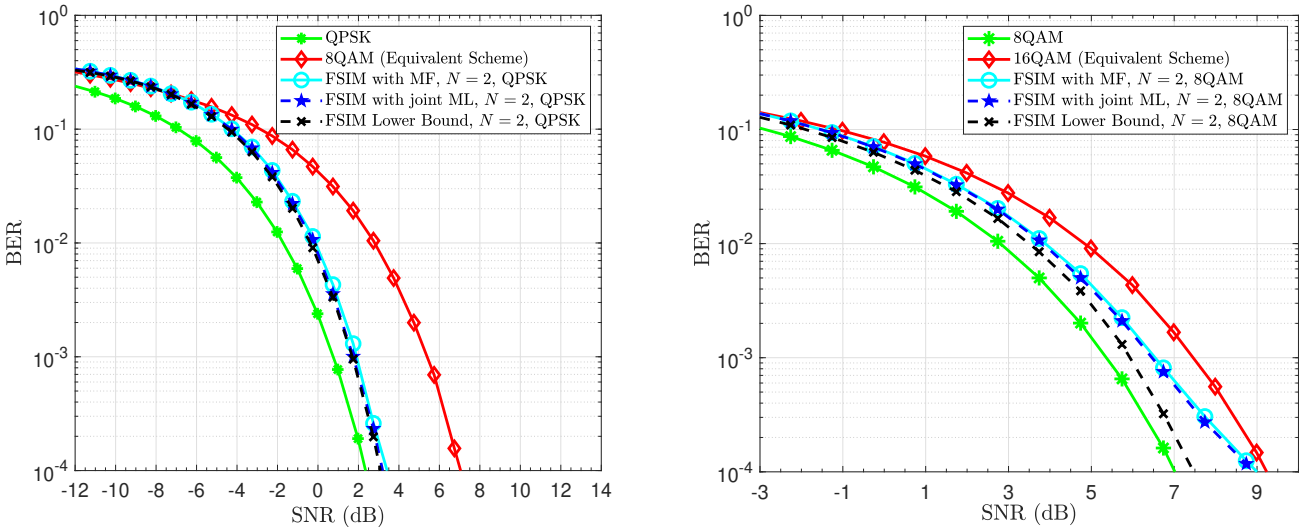

(a) (b)

Figure 9: Uncoded BER performance of 2-FSIM-MQAM, its analytical lower bound and its equivalent scheme $2M$QAM of the same SE: (a) 3 bits/symbol using $M = 4$, (b) 4 bits/symbol using $M = 8$.

minimum distance d_{min} between constellations), so a better ISI estimation and cancellation are achieved. Similarly, this probability with ISI estimation and cancellation using 2-FSIM-8QAM and 2-FSIM-16QAM is very tight to the lower bound at low SNR values, while the gap between them increases at high SNR values due to the residual ISI. In addition, it is clear that this degradation due to residual ISI is more important with higher M-ary QAM as shown with 2-FSIM-32QAM in Fig. 8b. This can be justified by the fact that higher M-ary QAM schemes are more sensitive to ISI (smaller d_{min}) compared to QPSK. Note that the two used filter shapes satisfy all the filter bank design requirements mentioned in sub-section 3.3, but they are not the optimal filters. Thus, the performance of FSIM can become tighter to the lower bound when the filter's bank shapes are optimally designed. Hence this analytical bound is a helpful indicator for evaluating the performance of the proposed system.

In the following, the proposed FSIM system is compared to the conventional transceivers under different configurations but with the same SE. The uncoded BER of these systems as a function of the average SNR is evaluated using Monte Carlo Simulations and theoretical lower bound according to (30). The comparison in Figs. 9a-10b is performed with ISI estimation and cancellation under an AWGN channel with MF and joint ML detectors. It should be highlighted that the theoretical BER lower bound (30) and the simulated BER with perfect ISI cancellation are very tight, and they are represented by a single curve named FSIM lower bound in Fig. 9a-10b. In addition, these figures show that the performance with the MF detector is very tight to that with the joint ML detector but with extremely lower complexity. The propagation of error issue clearly appears in Fig. 10b using both detectors (or any other) due to residual ISI from the error in tentative and feedback decisions in the preceding block for ISI estimation and cancellation. Thus, the error propagation is an issue with any detector, and it can be minimized by optimal filter design that allows mainly the correct tentative decisions.

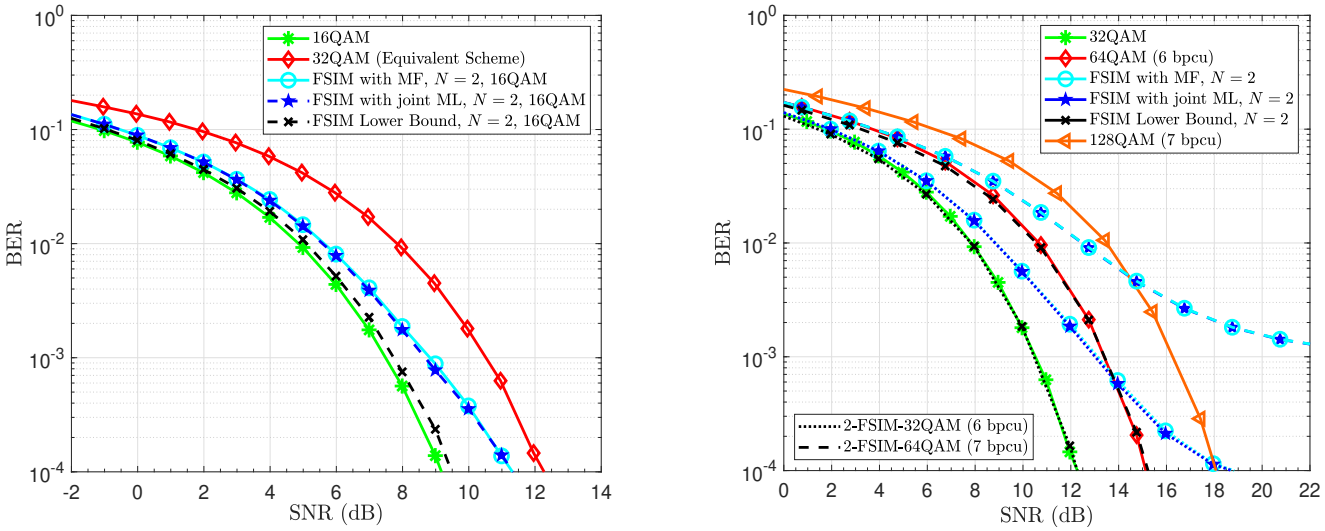

Figure 10: Uncoded BER performance of 2-FSIM-MQAM, its analytical lower bound and its equivalent scheme $2M$QAM of the same SE: (a) 5 bits/symbol using $M = 16$, (b) 6 and 7 bits/symbol using $M = 32$ and $M = 64$ respectively.

In order to conduct a fair comparison, the performance of the proposed system is compared to an equivalent conventional transceiver (M-ary QAM scheme with RRC filter) of the same SE. The system 2-FSIM-QPSK is depicted in Fig. 9a, where an important SNR gain of 3.8 dB is obtained at BER $= 10^{-4}$ compared to the equivalent 8QAM scheme. Accordingly, for the same BER performance, the SE enhancement by 1 bit/symbol requires an additional 0.9 dB only to the required SNR of QPSK. However, for the same SE enhancement with respect to 8QAM and 16QAM, an additional 2 dB is required with 2-FSIM-8QAM and 2-FSIM-16QAM as shown in Figs. 9b and 10a respectively. While the higher-order equivalent schemes as 16QAM and 32QAM need an additional 2.2 dB and 3.1 dB respectively instead of 2 dB with 2-FSIM-8QAM and 2-FSIM-16QAM. It is worth mentioning that a higher SNR gain is achieved when the proposed system, using two filters, is applied to a square QAM, so this system allows us to avoid the inherited performance degradation of non-square QAM by using FSIM with the lower square M-ary QAM order. In other words, as depicted in Fig. 9b the system 2-FSIM-8QAM has a smaller SNR gain due to the fact that the SNR gap between the performance of the non-square constellations of 8QAM and that of 16QAM is small for the same BER performance.

It is worth mentioning that these FSIM schemes are able to achieve SE and EE gain even with non-optimal filters compared to conventional APM schemes. In addition, this superiority is maintained when the FSIM is compared to existing single and dual-mode SISO-IM schemes of worse EE due to the need of higher power to maintain the same SE by using larger M-ary and/or to detect the transmitted VBs (see [43] and references therein).

For further analysis of the proposed scheme, the results with higher-order APM as 2-FSIM-32QAM and 2-FSIM-64QAM are presented in Fig. 10b, where their performance with ISI estimation and cancellation starts to degrade compared to equivalent schemes 64QAM and 128QAM respectively at high SNR values. It can be noticed that at low SNR, the

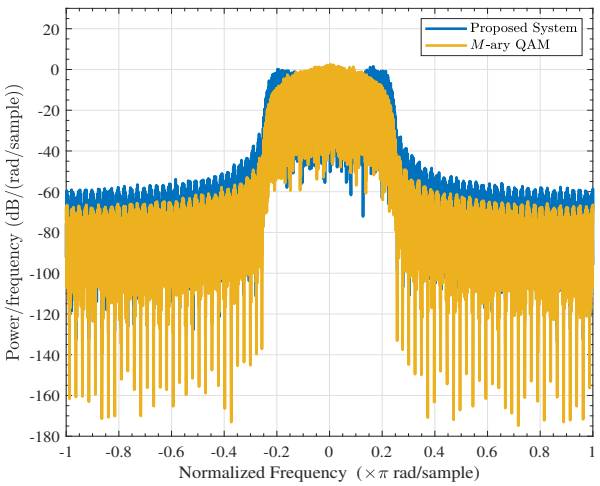

Figure 11: Spectrum comparison between the proposed FSIM system with 2 non-optimal filters and the conventional transceivers with QAM and RRC filters.

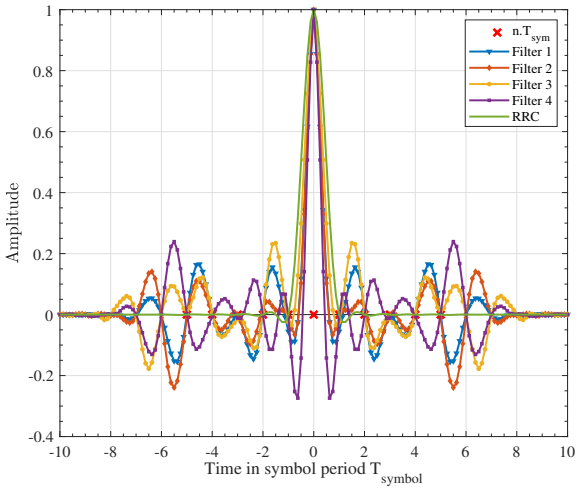

Figure 12: Complete responses of the 4 filters obtained after correct matched filtering at the receiver side, where $\eta = 10$ and $\lambda = 8$.

performance of the proposed systems with high M-ary APM is better than their equivalent schemes. An error floor appears with the higher-order M-ary APM caused by the residual ISI not completely mitigated by the receiver, and which has been induced by the non-optimal filters being used.

However, the BER of the latter two schemes with perfect ISI cancellation is very tight to the performance of 32QAM and 64QAM, respectively, while enhancing the transmission rate by 1 bit. Hence, this maximum achievable performance shows that there is always room for future improvements by designing an optimal filter bank and proposing better ISI mitigation techniques.

The spectrum of the conventional transceiver and the 2-FSIM-MQAM are compared in Fig. 11. It can be observed that most of the emitted power of both systems are concentrated on the same bandwidth. However, the OOB radiations of the proposed system is 10 dB higher than that of a conventional transceiver due to the fact the used filter f_2 has higher OOB radiation compared to f_1 and RRC filters.

By considering the filter bank design requirements mentioned in sub-section 3.3, a set of $N = 4$ filters is designed by using η and λ as mentioned in Table 2, and the complete filter response is depicted in Fig. 12. The mean of the signal to the introduced ISI power ratio for all possible filter sequence permutations is 26.29 dB, and the dot-product symmetric matrix between these non-optimal filters is:

$$\mathbf{\Xi} = \begin{bmatrix} 1 & 0.7615 & 0.7284 & 0.334 \\ 0.7615 & 1 & 0.6376 & 0.0887 \\ 0.7284 & 0.6376 & 1 & 0.67 \\ 0.334 & 0.0887 & 0.67 & 1 \end{bmatrix}$$

The results using these 4 filters with QPSK and 16QAM is depicted in Fig. 13a and Fig. 13b, where 4-FSIM-QPSK (4-FSIM-16QAM) has 1.7 (2.2) dB gain compared to its equivalent

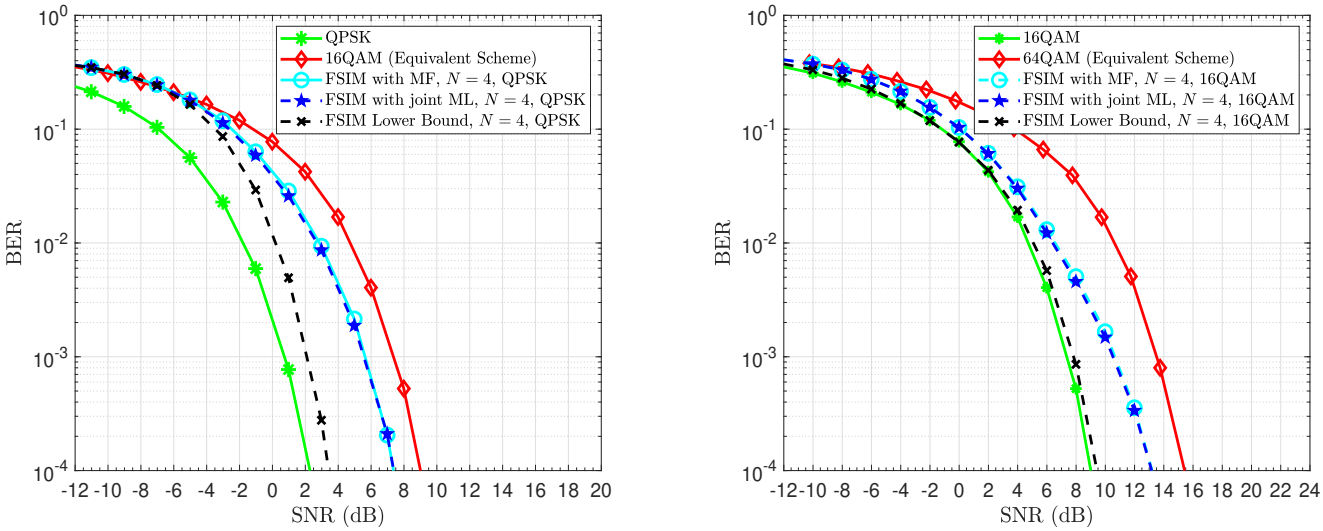

(a) (b)

Figure 13: Uncoded BER performance of 4-FSIM-MQAM, its analytical lower bound and its equivalent scheme 4MQAM of the same SE: (a) 4 bits/symbol using $M = 4$, (b) 6 bits/symbol using $M = 16$.

scheme 16QAM (64QAM). Note that 4-FSIM-QPSK (4-FSIM-16QAM) requires 3.9 (3.6) dB more than its lower bound due to high dot-product between some filters.

After presenting these encouraging FSIM scheme results, its uncoded BER vs E_s/N_0 (E_s is the energy per symbol) is evaluated and compared in a frequency selective fading channel to the competitors SC schemes in single and dual-mode. A Rayleigh fading channel is considered with J-paths of an integer multiple of symbol period delays, and the MMSE-FDE is used for all schemes of the same SE (DM-SC-IM, SC-TIM and their Reduced Correlation (RC) versions with interleaver [13]). Note that the optimal joint ML detector is used for these schemes, while a MF-based detector of lower complexity is used for FSIM. The frame setup in symbol length is: $N_s = 1015, N_{ZP} = N_{CP} = 9$, and the schemes' configuration, to have average SE$\approx$ 3 bits/symbol, are: (RC-)SC-TIM: $M = 16, N_a = 3, N_g = 5, G = 203$, (RC-)DM-SC-IM:$M_A = 8, M_B = 4, N_a = 2, N_g = 5, G = 203$, and FSIM: $M = 4, N = 2$. Figs. 14a-14b show clearly that FSIM with ISI estimation and cancellation outperforms all other schemes with a minimum gain of 6 dB (4.2 dB) compared to the second-best scheme RC-SC-TIM in Rayleigh selective channel with $J = 2$ ($J = 4$).

Furthermore, we would like to mention that the proposed system can achieve better performance and a higher EE gain by using an optimal filter bank satisfying the requirement discussed in Section 3.3. Note that the design of a larger filter bank ($N > 4$) is a challenging and open research problem that goes beyond the scope of this work, and solving this problem will certainly lead to better SE gain.

3.6 FSIM vs Media-Based Modulation

Finally, to avoid any ambiguity between the filter IM domain and existing IM schemes, it is interesting to highlight the differences between the proposed filter domain and the

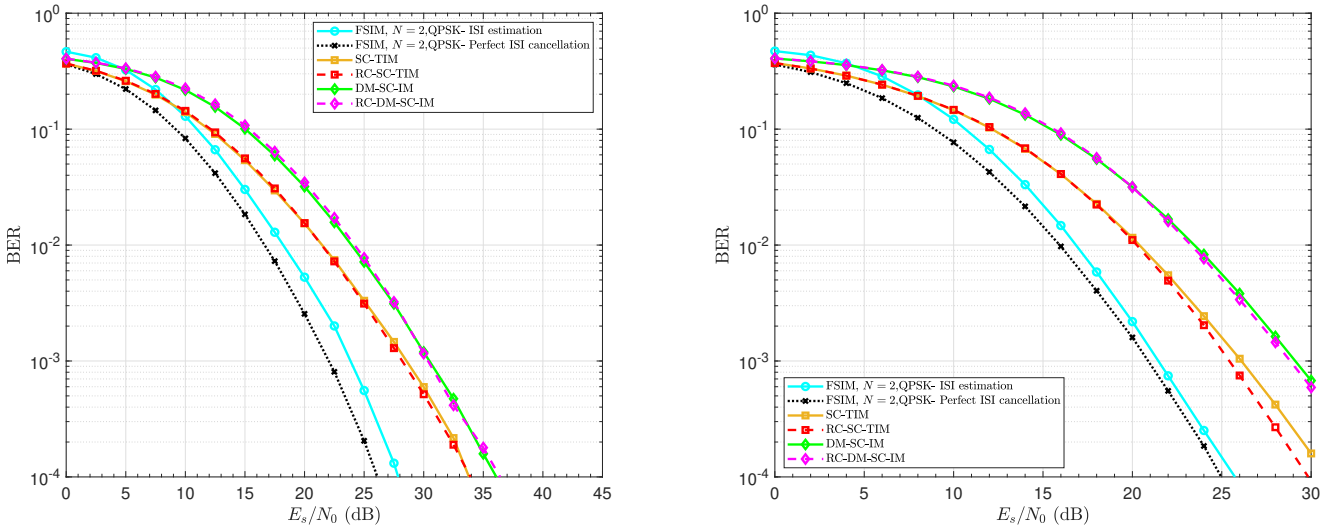

Figure 14: Average uncoded BER comparison of different SC schemes with IM in a frequency selective Rayleigh fading: (a) $J = 2$, (b) $J = 4$.

Media-Based Modulation (MBM) IM scheme [47]. The main similarities/differences between proposed FSIM-MIMO and the SISO-MBm are extracted and summarized as follows:

- FSIM uses N filter shapes to convey $log2(N)$ additional information bits, while MBM uses $N_{RFmirrors}$ to generate different channel states and convey $N_{RFmirrors}$ additional information bits as long as the independence of the generated radiation patterns is guaranteed.
- For high data rates system, the design of SISO-MBM schemes with such high number of RF mirrors (different states) is a challenging research problem because it needs to jointly optimize the radiation-related parameters, such as reflection coefficient, antenna gain, radiation efficiency, and so on.
- FSIM is not based on any channel condition, whereas MBM requires rich scattering environment (Non Line-of-Sight (LoS) Rayleigh Channel) and it is very challenging task in LoS scenario to obtain sufficiently independent fade realizations for MBM systems [48].
- In contrary to FSIM, SISO-MBM has an inherent diversity gain due the superposition of the same transmitted symbol from the different reflections caused by $N_{RFmirrors}$ RF mirrors. Note that SISO-MBM allows using a single RF chain while achieving some diversity gain, and it is very similar in SE enhancement to ExSSK [49] with the number of transmit antennas $N_t = N_{RFmirrors}$.
- For the same SE, MBM provides a significantly better error performance compared to traditional M-ary modulated systems since the Euclidean distance between MBM constellation points, which are random fade realizations, remains the same even with

increasing SE values. The advantage of MBM further increases for higher order constellations and a higher number of receive antennas [48]. However, this gain is achieved only where more than one receive antenna (SIMO mode) is used as shown in Fig. 4 of [48] and it is one of the main listed disadvantages that states the MBM performance is not satisfactory for a small number of receive antennas. Whereas the results of FSIM shows that a significant gain is achieved even using non-optimal filters in SISO mode especially with low order modulations.

- FSIM requires the channel estimation using limited number of pilots or training sequence only with any number of filters, whereas the main shortcomings of the MBM system is the excessive channel sounding burden. In order to obtain the CSI, the receiver has to be trained with pilot signals from all possible antenna states, that is, $2^{N_R Fmirrors}$ test signals are required for a single reconfigurable antenna.

3.7 Conclusion

Index Modulation is explored in the spatial, temporal, and frequency domain. In this Section 2 , we propose a novel domain for IM, named the "Filter domain" and a novel scheme "Filter Shape Index Modulation" where the index of the filter is used at the transmitter to convey additional information bits and enhance the SE by $\log_2 N$. Note that this domain allows a SE enhancement by at least 1 bit/s/Hz in contrast to the existing domains in SISO (temporal and frequency domains) where their maximum enhancement is limited to 0.6 bit/s/Hz or less.

This novel domain is investigated by proposing the FSIM system, where a bank with different filter shapes is used. In addition, the joint ML detector that detects the filter index and the transmitted APM symbol is presented. Then, a low complexity optimal detection scheme based on a Matched filter is proposed. Moreover, an ISI cancellation process is proposed due to the fact that FSIM introduces a controlled ISI. Note that the proposed system can be reconfigured to act as a conventional transceiver by using the same Nyquist filter for all symbols.

The theoretical lower bounds for filter error probability and BER are derived, and the analysis validates the achieved performance using the proposed FSIM approach. Monte Carlo simulations showed that the FSIM-QPSK system with 2 and 4 non-optimal filters offers, at BER= 10^{-4} and same SE, a gain of 3.8 dB and 1.7 dB as compared to their equivalent systems 8QAM and 16QAM, similarly, 4-FSIM-16QAM achieves a gain of 2.2 dB. It is worth mentioning that FSIM maintains its superiority in a frequency selective channel compared to existing SC SISO-IM schemes where the former achieves a minimum gain of 4 to 6 dB. Thus, the proposed scheme demonstrates that ISI is not necessarily undesirable while it is controllable and predictable, since it permits to achieve a higher system capacity compared to systems that enforce zero interference. Finally, it can be concluded that FSIM scheme can achieve even higher SE after designing a larger filter bank (higher N), and it is useful for ultra-high rate wireless communication.

4 Proposed MIMO SMX-FSIM system

4.1 Introduction

A generalized SMX system is proposed in this Section 4 motivated by the different advantages of FSIM scheme and its generalizations for various existing IM schemes. Thus, this system includes different existing schemes as special cases (e.g., SMX with conventional APM, MIMO-OFDM-IM [10], and SMX with any time/frequency IM), since filter IM domain can be configured to change the emitted symbol [3]. The transmission of different FSIM symbols from the TAs allows achieving a higher SE and EE gain. In other words, any small SE enhancement by FSIM in SISO has a tremendous impact when it is extended to MIMO system, where the overall SE gain by SMX FSIM compared to SMX QAM is $N_t \log_2 N$ for $N_t \leq N_r$. In addition, a simple receiver for SMX-FSIM is presented in this Section 4, where a sample level equalization is performed, and followed by a parallel Matched Filter (MF) based detector. Moreover, the theoretical system performance is derived and validated by Monte Carlo simulations and then compared with other equivalent systems.
The main contributions in Section 4 are summarized as follows:

1. A generalized MIMO SMX system is proposed by incorporating FSIM scheme to achieve high SE and EE gain. The proposed SMX-FSIM system conveys information bits in the signal and filter IM domains. The VBs are encapsulated by the different filter shapes indices that are used for pulse shaping of the N_t simultaneously transmitted APM symbols. Note that the transmit spatial IM (e.g., GSM system) conveys all the VBs by a single index (index of activated TAC), and its misdetection leads to bit errors in most of the VBs and also in the real bits of all transmitted APM symbols (i.e., N_a APM symbols in GSM will be most probably mis-detected when an error occurs in the TAC index detection). However, the decentralization of VBs encapsulation in SMX-FSIM avoids the highlighted single point of failure in GSM system.

2. A simple receiver for SMX-FSIM is presented, which is based on Zero-Forcing (ZF) sample level equalizer followed by a parallel MF-based detector. The proposed parallel detection for SMX-FSIM provides good performance with prominent complexity reduction compared to the joint Maximum Likelihood (ML)-based detector.

3. The analytical performance of SMX-FSIM using ZF equalizer is derived and validated by Monte Carlo simulations. Then, they are compared to those of the conventional SMX QAM system of the same SE. The results show an important SE and EE gain can be achieved even with a low number of filter shapes.

4. The performance of the proposed SMX FSIM scheme is evaluated under sub-THz channels with RF impairments, then compared to the existing ultra-high data rate candidates (GSM and conventional SMX QAM [22]).

5. These sub-THz candidates are compared and analyzed from different perspectives (performance, robustness to PN, SE/EE, cost, PAPR, and power consumption). The results reveal that the spectral-efficient SMX-FSIM system with power-efficient APM is the best promising candidate for such systems in sub-THz bands because it has better performance and robustness to PN, higher SE and EE gain, lower power consumption

and cost, as well as it avoids the RF switching problem that appears with transmitter spatial IM (e.g., GSM).

4.2 System Model

In the design of the novel FSIM based MIMO transceiver and its analysis, we considered most of the sub-THz band's peculiarities. In particular, the following points related to technological limitations, RF impairments, and sub-THz channel characteristics are considered in the waveform and system design phase:

- Low output transmit output power with limited achievable SNR [22]. Thus, the new sub-THz waveform should be energy efficient to maintain good performance.
- Important RF impairments such as carrier frequency offset (CFO) and phase noise of the oscillator that increase at higher frequencies [50]. The CFO can be estimated and canceled, but the PN's dominant term in a wide sub-THz band that cannot be completely compensated is the random Gaussian process. This random term of the PN has the highest impact on performance degradation [51]. Thus, a waveform robust to PN is required to maintain a good performance with the residual PN.
- A low data converters resolution (quantization levels) is preferred to avoid the high cost and power of the ultra-high sampling rate data converters (ADC/DAC) with high resolution.

Therefore, in our approach to design the proposed novel MIMO transceiver, we insist on using a power-efficient single carrier modulation with low order modulation to provide better robustness for sub-THz bands and survive with these limitations. However, to reach ultra-high data rates in the order of Terabits per second, a spectral efficient IM technique is required even with the large available bandwidth, and thus we exploited our novel Index Modulation domain "Filter IM domain". The proposed system will enhance the SE by exploiting all available time, frequency, and spatial resources in contrast to most IM domains. Moreover, the proposed SMX-FSIM transceiver will also enhance the EE because the VBs, in general, can be detected at lower SNR, as it will be confirmed at the end of this deliverable.

4.2.1 SMX FSIM Transmitter

Consider a $N_t \times N_r$ MIMO-SMX system ($N_t \leq N_r$), where N_t and N_r are the number of transmit and receive antennas respectively. In this paper, FSIM scheme that conveys information bits by the index of the different filter shapes and the APM symbols is considered to achieve high SE and EE gain. Note that this system SMX-FSIM in the filter IM domain allows to use all available resources in contrast to other IM domains (time, frequency, antennas, etc.).

The input bitstream b is divided into N_t sub-streams $b_1, b_2, ..b_{N_t}$, as shown in Figure 15, and passed through its corresponding FSIM modulator.

Each sub-stream b_j contains the real and virtual information bits denoted by b_j^R and b_j^V respectively. The former is mapped using the M-ary APM (e.g., QAM, PSK), while the latter is translated to an index i^j, which represents the index of the selected filter f_{i^j} at the j^{th} TA. Then, the APM symbol c^j is pulse shaped, as depicted in Fig. 16, using the filter $f_{i^j}[m]$ of length L samples with m is the sample index from 0 to $L-1$. Note that the filter

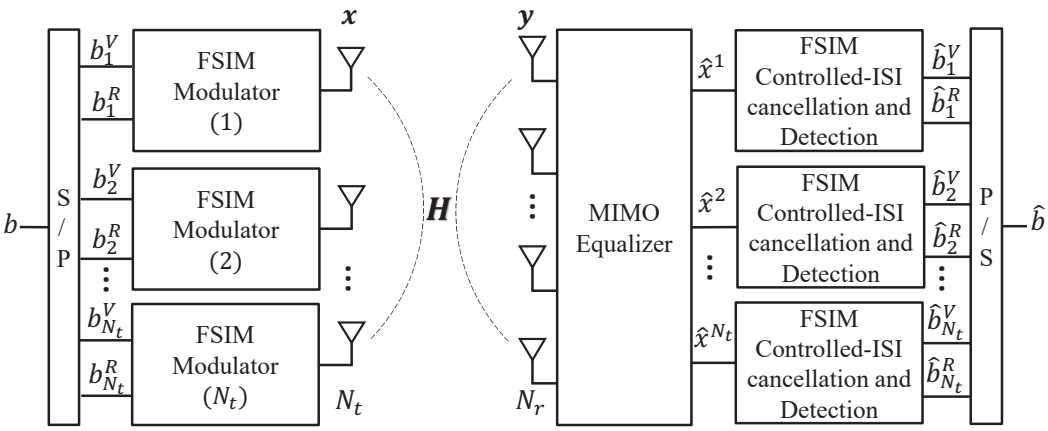

Figure 15: System model of $N_t \times N_r$ SMX-FSIM transceiver.

is truncated in the time domain to η APM symbols, and it is sampled at a rate of λ samples per symbol, which yields $L = \eta.\lambda + 1$. Then, the FSIM modulators' outputs are transmitted simultaneously from the N_t TAs.

The filter bank for each FSIM modulator shown in Fig. 16 includes N different filter shapes where N is a power of 2. Without loss of generality, we consider that SMX-FSIM uses the same filter bank and APM for all TAs. Subsequently, the total number of bits per SMX-FSIM symbol $\mathrm{SE}_{\text{SMX-FSIM}}$ can be expressed as:

$$\begin{aligned} \mathcal{L}_{\text{SMX-FSIM}} &= N_t(\log_2 N + \log_2 M) \\ &= N_t \log_2 N + \mathcal{L}_{\text{SMX-QAM}}, \end{aligned} \tag{31}$$

where $\mathcal{L}_{\text{SMX-QAM}} = N_t \log_2 M$ is the number of transmitted bits of a conventional MIMO-SMX system with N_t TAs and M-ary APM. It is clear that the SE gain increases linearly with the number of TAs, and it is $N_t \log_2 N$ higher than that of the conventional MIMO-SMX system with the same M-ary APM.

The output of the filter bank $s_n^j[m]$ for the n^{th} APM symbol c_n^j at the j^{th} TA is:

$$s_n^j[m] = \left(f_{i_n^j} * c_n^{j\prime}\right)[m] = c_n^j f_{i_n^j}[m], \tag{32}$$

where $c_n^{j\prime}$ is the up sampled copy of c_n^j by a factor L.

Then, the signals $s_n^j[m]$ are passed through the Overlap and Add (OLA) block as shown in Fig. 16 to generate the emitted signal $x_n^j[p]$ as follows:

$$x_n^j[p] = \sum_{n'=n-\lceil \eta/2 \rceil}^{n+\lfloor \eta/2 \rfloor} s^j{}_{n'}[p - (n' - n)\lambda], \tag{33}$$

where the index $p = p_{\text{center}} - \lceil \lambda/2 \rceil + 1, ..., p_{\text{center}} + \lfloor \lambda/2 \rfloor$ and the index of the middle desired sample is $p_{\text{center}} = \frac{L-1}{2}$ [3]. Note the used filters introduce Inter-Symbol Interference (ISI) since Nyquist condition for zero ISI is relaxed in FSIM scheme to achieve higher SE by indexing distinguishable filter shapes.

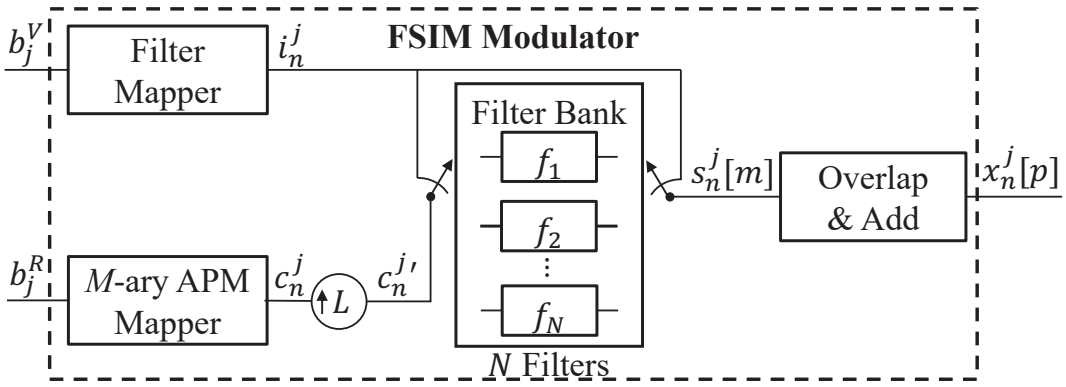

Figure 16: System model of FSIM Modulator with M-ary APM mapping and a filter bank of N filters.

4.2.2 SMX FSIM Receiver

At the receiver, the received signal in time domain $\mathbf{y}$ can be expressed as:

$$\mathbf{y} = \mathbf{H}\mathbf{x} + \mathbf{v}, \tag{34}$$

where $\mathbf{H} = [\mathbf{h}_1, ..., \mathbf{h}_{N_t}]$ is the $N_r \times N_t$ MIMO channel matrix with $\mathbf{h}_i$ is the column vector of N_r elements, $\mathbf{x} = [x_1, \ldots, x_{N_t}]^T$ is the transmitted vector that contains N_t different FSIM symbols, $\mathbf{v}$ is $N_r \times 1$ channel noise vector and its v_r elements are complex Gaussian variables, Identically Independent Distributed (i.i.d.), with zero-mean and variance σ^2, i.e, $\mathcal{CN}(0, \sigma^2)$ for $r = 1, \ldots, N_r$.

Equalization: The received signal suffers from Inter-Antenna Interference (IAI) and inter-symbol interference due to the MIMO transmission and the used non-Nyquist filters in FSIM scheme respectively. In other words, the former represents the interference from simultaneously transmitted symbols from other antennas, while the latter is the interference contribution from the previous and the future symbols emitted from the same antenna (within a filter period). When the receiver intends to detect the j^{th} FSIM symbol transmitted from the j^{th} TA, the received signal can be rewritten as follows to highlight the IAI components :

$$\mathbf{y} = \mathbf{h}_j x^j + \sum_{l=1, l\neq j}^{N_t} \mathbf{h}_l x^l + \mathbf{v}. \tag{35}$$

In addition to IAI, the symbols suffer from ISI due to filters used at the transmitter that do not satisfy Nyquist ISI criterion. At the first stage in receiver side, the received signal is passed through an equalizer to eliminate the effect of the channel $\mathbf{H}$. Note that ZF or Minimum Mean-Square Error (MMSE) equalizers can be used, or any other equalizer that conserves the FSIM filter contribution. Here the equalization is performed at sample level before matched filter and down-sampling and not at symbol level as usual, since the pulse shaping filter used at the transmitter is still unknown at this stage. In the following, the linear ZF equalizer is adopted to eliminate channel effect on all received samples and allow the detection of the transmitted FSIM symbol (APM symbol and index of the used filter). Then the output of the equalizer can be written as follows:

$$\hat{\mathbf{x}} = \mathbf{W}\mathbf{y} = \mathbf{x} + \mathbf{W}\mathbf{v}, \tag{36}$$

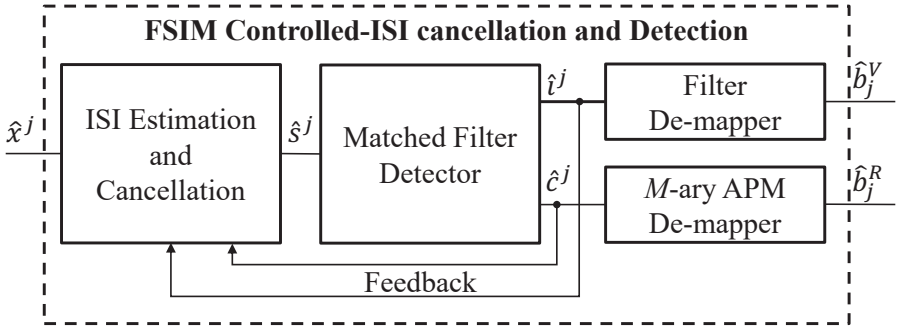

Figure 17: System model of FSIM demodulator with the controlled-ISI cancellation and detection.

where $\hat{\mathbf{x}}$ is the vector of equalized samples and $\mathbf{W} = [\mathbf{w}_1^T, \mathbf{w}_2^T, \ldots, \mathbf{w}_{N_t}^T]^T$ is the ZF weight matrix expressed as:

$$\mathbf{W} = (\mathbf{H}^H\mathbf{H})^{-1}\mathbf{H}^H, \tag{37}$$

and $\mathbf{w}_j$ is the j^{th} row of $\mathbf{W}$.

Afterward, in order to have an effective detection of the transmitted FSIM symbol (filter index and APM symbol), the estimation and cancellation of the controlled-ISI from the used non-Nyquist filters is performed in parallel as shown in Fig. 15 on the equalized stream of samples $\hat{x}^j$ similar to the simplified SISO FSIM receiver depicted in Fig. 17.

Hence, the samples stream $\hat{x}^j$ corresponding to the j^{th} TA is passed to the ISI Estimation and Cancellation block [3], that intends to remove the ISI generated from the used filters that do not satisfy Nyquist zero-ISI criterion. The output of the ISI Cancellation block can be expressed as follows:

$$\hat{s}_n^j[m] = c_n^j f_{i_n^j}[m] + ISI_{resid}^j[m] + \mathbf{w}_j\mathbf{v}[m], \tag{38}$$

where the $ISI_{\text{resid}}^j[m]$ represents the residual ISI that might still persist due to the non-perfect ISI cancellation.

Then, for each $j = 1, \ldots, N_t$, the ISI cancellation output signal $\hat{s}_n^j[m]$ is passed through a MF-based detector to estimate the APM symbol and the index of the selected filter at the j^{th} TA.

Detection: In the following, the detection of the APM symbol and filter index is considered for one TA, since all TAs perform in parallel a similar detection. Each MF-based detector contains a bank of N matched filters g_k where $g_k(t) = f_k(T_f - t)$ with $0 \leq t \leq T_f$, $T_f = L.T_s$ and T_s is the sampling period [3]. The output of these filters r_k^j sampled at the instant T_f can be expressed as follows:

$$r_k^j = \int_0^{T_f} \hat{s}^j(\tau) f_k(\tau) d\tau, \quad k = 1, 2, ..., N. \tag{39}$$

Then, the selected filter at the transmitter side on the j^{th} TA can be recovered by taking the maximum energy of the sampled MF outputs r_k^j as follows:

$$\hat{\imath}^j = \arg\max_k \|r_k^j\|^2. \tag{40}$$

After estimating the index of the filter being used at the j^{th} TA, the APM symbol detection is performed on $r_{\hat{i}^j}$. Afterwards, the detected symbols $\hat{c}^j$ and filter index $\hat{i}^j$ are passed to their corresponding demappers to recover the sub-streams $\hat{b}_j^R$ and $\hat{b}_j^V$ respectively. The above mentioned steps are processed in parallel for the N_t transmitted FSIM symbols, and finally the parallel to serial recovers the bitstream $\hat{b}$ as depicted in Fig. 15.

4.3 Theoretical Performance

In this section, the analytical lower bound in terms of Symbol Error Rate (SER) for the proposed system SMX-FSIM is derived, where we consider that the ZF equalizer and the parallel MF-based detector are used. The system performance of SMX-FSIM depends on the APM symbols and filter index detection. In addition, the lower bound theoretical SER and BER are deduced under the assumption of perfect ISI cancellation (*i.e.* $ISI_{resid} = 0$), and near-orthogonal filter shapes that can be achieved when the filter bank is well designed.

After the linear equalization according to (36), the output of the matched filter bank at j^{th} TA sampled at $t = T_f$ given by r_k^j in (39) can be rewritten as:

$$\begin{aligned} r_k^j &= \langle \mathbf{f}_k, \mathbf{f}_{i_n^j} \rangle . c_n^j + \langle \mathbf{f}_k, \mathbf{w}_j \mathbf{v}_n \rangle \\ &= \begin{cases} c_n^j + \langle \mathbf{f}_k, \mathbf{w}_j \mathbf{v}_n \rangle & \text{for } k = i_n^j \\ \langle \mathbf{f}_k, \mathbf{f}_{i_n^j} \rangle . c_n^j + \langle \mathbf{f}_k, \mathbf{w}_j \mathbf{v}_n \rangle & \text{for } k \neq i_n^j, \end{cases} \end{aligned} \tag{41}$$

where $\mathbf{v}_n$ are the L samples around the n^{th} symbol.

The detection of the filter index $\hat{i}^j$ at the j^{th} TA is estimated according to (40) by choosing the maximum $U_k = \|r_k^j\|^2$ which represents the energy of r_k^j . Note that U_k follows the independent non-central Chi-Square distribution [45] for all k with degree of freedom equal 2 and the non-central parameter α^2 that can be expressed as follows:

$$\alpha_{k,q}^2 = \begin{cases} \|c_n^j\|^2 = \mathcal{E}_q & for\, k = i_n^j \\ \langle \mathbf{f}_k, \mathbf{f}_{i_n^j} \rangle^2 . \|c_n^j\|^2 = \langle \mathbf{f}_k, \mathbf{f}_{i_n^j} \rangle^2 . \mathcal{E}_q & for\, k \neq i_n^j, \end{cases} \tag{42}$$

where $f_{i_n^j}$ is the selected filter at the j^{th} TA and $\mathcal{E}_q$ is the transmitted energy of the APM symbol c_n^j.

Therefore, the PDF of U_k can be written as follows:

$$p(u_k) = \frac{1}{2\sigma_p^2} e^{-\frac{u_k + \alpha_k^2}{2\sigma_p^2}} \mathcal{I}_0 \left(\frac{\alpha_k \sqrt{u_k}}{\sigma_p^2} \right), \tag{43}$$

where $u_k \geq 0$, σ_p^2 is the post-equalization noise variance, and $\mathcal{I}_0(\rho)$ is the zero order modified Bessel function of 1^{st} kind given by (20) [45].

Since the MF-based detector for all $j = 1, \ldots, N_t$ performs APM and filter index estimation in parallel for all TAs similar to SISO-FSIM detection [3], we will consider the detection on one of the TA, and the index j is omitted. Let us suppose that the filter f_1 is selected at the transmitter side for the APM symbol c_n. The detector makes a correct index decision; if the probability of u_1 is greater than all other $N-1$ u_k values for $k \neq 1$. The filters are considered orthogonal to derive the lower bound, and thus the u_k become statistically independent, then the joint probability can be factorized as a product of $N-1$ marginal probabilities of

the form as shown in (22). Similarly, the probability of a correct decision is given by (23) [3], and the probability of a filter index error can be deduced from probability of a correct decision as in Subsection 3.4- Eq. (24). The average probability of filter index error ought to be the weighted average filter error accross the Q possible energy levels of APM symbols, given as follows:

$$P_{e,filter} = \sum_{q=1}^{Q} P_{e,\mathcal{E}_q}.P(\mathcal{E}_q), \tag{44}$$

where $P(\mathcal{E}_q)$ is the probability of occurrence of the energy level $\mathcal{E}_q$. The SER of M-ary QAM modulation in AWGN channel is given by [45]:

$$P_{e,QAM} = \begin{cases} 4\left(1-\frac{1}{\sqrt{M}}\right)Q\left(\sqrt{\frac{3}{M-1}SINR}\right) & \text{k is even} \\ \quad -4\left[\left(1-\frac{1}{\sqrt{M}}\right)Q\left(\sqrt{\frac{3}{M-1}SINR}\right)\right]^2 & \\ \left(\frac{4IJ-2I-2J}{M}\right)Q\left(\sqrt{\frac{6log_2(IJ)}{(I^2+J^2-2)}SINR}\right) & \text{k is odd} \\ \quad -\frac{4}{M}\left(1+IJ-I-J\right)Q^2\left(\sqrt{\frac{6log_2(IJ)}{(I^2+J^2-2)}SINR}\right), & \end{cases} \tag{45}$$

where $SINR$ is Signal-to-Interference-plus-Noise Ratio, Q is the Q-function, $k = \log_2 M$, $I = 2^{\frac{k-1}{2}}$, and $J = 2^{\frac{k+1}{2}}$.

Subsequently, the correct detection of FSIM symbols arises when both the filter and the APM symbol are correctly estimated, therefore the probability of a correct FSIM decision at a given TA is $(1 - P_{e,filter})(1 - P_{e,QAM})$ and the SER_{FSIM} is given by:

$$SER_{\text{FSIM}} = 1 - (1 - P_{e,filter})(1 - P_{e,QAM}). \tag{46}$$

Then, the SINR estimation at the j^{th} branch can be written as:

$$SINR_j = \frac{\mathbb{E}\{\hat{s}_j^2\}}{\mathbb{E}\{\mathbf{w}_j\mathbf{v}_n\}} = \frac{P}{\|\mathbf{w}_j\|^2\sigma^2} = \frac{SNR}{\|\mathbf{w}_j\|^2}, \tag{47}$$

where P is the average power on each TA, and SNR is the average transmitted signal to noise ratio.

We defined $\omega_j = 1/\sqrt{\|\mathbf{w}_j\|^2}$, then ω_j meets general Rayleigh distribution with variance $1/2$ and degree of freedom $2(N_t - N_r + 1)$ when the channel matrix $\mathbf{H}$ follows Rayleigh distribution. In this case, the probability density function (PDF) of ω_j is the following:

$$p_\omega(\omega_j) = \frac{2}{(N_r - N_t)!}(\omega_j)^{2(N_r-N_t)+1}e^{-(\omega_j)^2}. \tag{48}$$

In the ZF algorithm, the FSIM symbol detection is implemented independently on each branch of the equalizer output corresponding to the symbol emitted from the j^{th} TA with same configuration (filter bank, APM scheme and order), and the SINR of each sub data stream follows the same distribution with the same degree of freedom. Hence, the average

SER of SMX FSIM symbol with ZF and MF based detector receiver can be obtained under any fading channel as follows:

$$\begin{aligned} \mathrm{SER}_{\text{SMX FSIM}} &= \frac{1}{N_t}\sum_{j=1}^{N_t}(\mathrm{SER}^{j}_{\text{SMX FSIM}}) = \mathrm{SER}^{j}_{\text{SMX FSIM}} \\ &= \int_0^{\infty} SER_{FSIM}(\omega_j)p_{\omega}(\omega_j)d\omega_j, \end{aligned} \tag{49}$$

where the PDF $p_{\omega}(\omega_j)$ depends on the considered channel distribution.

4.4 Results and Discussions

After considering the sub-THz aspects in the design phase of the proposed SMX-FSIM system and its theoretical performance derivation, we validated these results firstly in this sub-section, and then we discussed and analysed the proposed MIMO SMX-FSIM system from different perspectives. Note that the detailed study of the proposed transceiver in MIMO sub-THz channels that are generated from a ray-based deterministic channel model by our BRAVE partner [52] and with RF impairments is presented in our deliverable D3.1 [5].

In this sub-section, we evaluated our proposed system SMX-FSIM using the derived theoretical performance in a Rayleigh channel. Several Monte Carlo simulations are performed to validate the theoretical lower bound SER performance (49) and compared to equivalent system of the same SE. Note that the theoretical SER performance of SMX-QAM with ZF equalizer is according to [53, Eq. (9)]. In addition, the SMX-FSIM system is compared at different transmission rates to its equivalent SMX-APM systems. For a fair comparison, both systems with ZF equalizer are compared with same number of receive antennas and under the same SE, which requires either the same modulation schemes with SMX-FSIM and SMX-QAM or the same number of transmit antennas. We cannot conserve the same values for both variables because SMX-QAM needs to accommodate the virtual bits conveyed in the filter IM domain by increasing one of these parameters. The simulation parameters for all configurations in this section are summarized in Table 3.

Table 3: Simulation parameters for MIMO FSIM and QAM based systems.

Parameters	Value
N_t for SMX-8QAM, SMX 2-FSIM-QPSK	$[4, 8, 10]$
N_t for SMX-QPSK	$[6, 12, 15]$
N_r	$[8, 12, 16]$
η	10
Oversampling factor: λ	8
Filter's length: L	81
Pulse shaping filter for Conventional Transceiver	Root Raised Cosine (RRC)
Number of channel realizations	500
Total Number of symbols	5×10^6

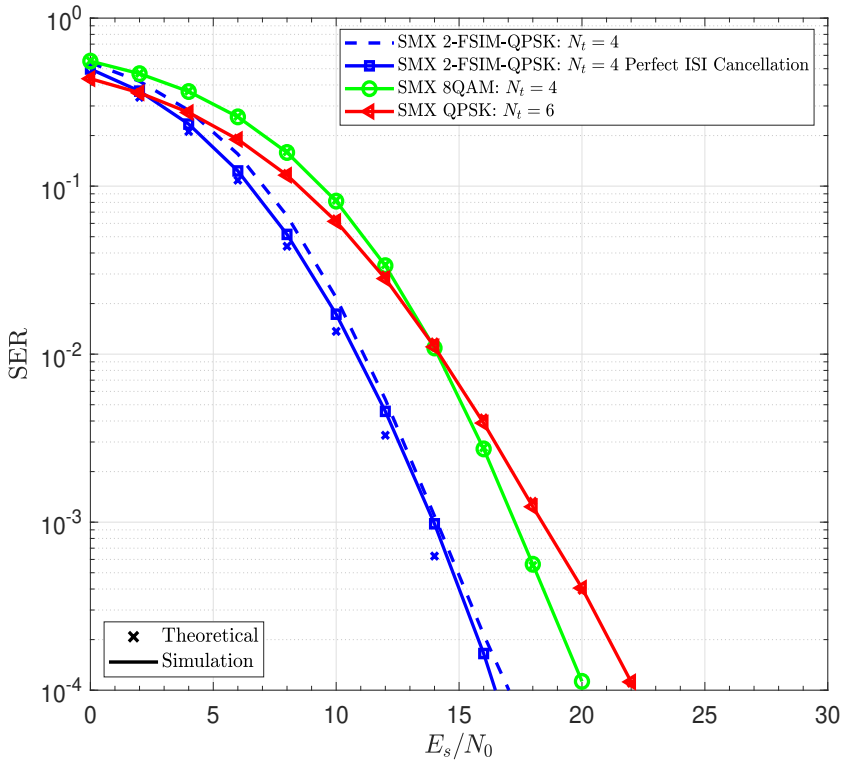

Figure 18: SER performance of the proposed SMX 2-FSIM-QPSK system and its equivalent SMX-QAM systems of same SE= 12 bpcu and $N_r = 8$.

Figures 18-20 show the SER performance for SMX-QAM and SMX-FSIM with/without perfect ISI cancellation in Rayleigh channel by transmitting 12 to 30 bits per MIMO symbol (or bit per channel use (bpcu)). In addition, the theoretical SER for both systems are compared to the Monte Carlo simulation results. The notation $N-$FSIM-APM is used to describe FSIM scheme with N filters and M-ary APM modulation schemes.

The different systems with 12 bpcu and $N_r = 8$ are: SMX-QPSK with N_t =6, SMX $2-$FSIM-QPSK and SMX 8QAM with $N_t = 4$. As we can notice that when we are using the same QAM order M for SMX-FSIM and SMX-QAM, N_t for the SMX-QAM system is larger to have the same SE. Similarly, when the same N_t is used, the modulation order is increased for SMX-QAM for same reason. The SER performance of these systems are depicted in Fig. 18, and it is clear that SMX 2-FSIM-QPSK system has 3 dB and 5.2 dB performance gain at SER= 10^{-4} compared to the equivalent SMX-8QAM and SMX-QPSK systems respectively.

Similar comparisons with larger number of transmit antennas are provided to achieve higher SE. The results in Figs. 19-20 show that SMX 2-FSIM-QPSK with $N_t = 8$ (SE=24 bpcu) and $N_t = 10$ (SE=30 bpcu) achieve around 3-3.5 dB performance gain compared to SMX-8QAM with same number of transmit antennas and more than 12 dB gain compared to SMX-QPSK.

Finally, it is worth mentioning that the simulated SER for SMX-QAM matches their theoretical curves, and the simulated SER for SMX-FISM system with perfect ISI cancellation is very tight to its theoretical lower bound in all configurations. Whereas, a slight performance degradation (less than 0.8 dB) can occur when using the proposed ISI estimation and cancellation technique due to residual ISI from the non-Nyquist filters.

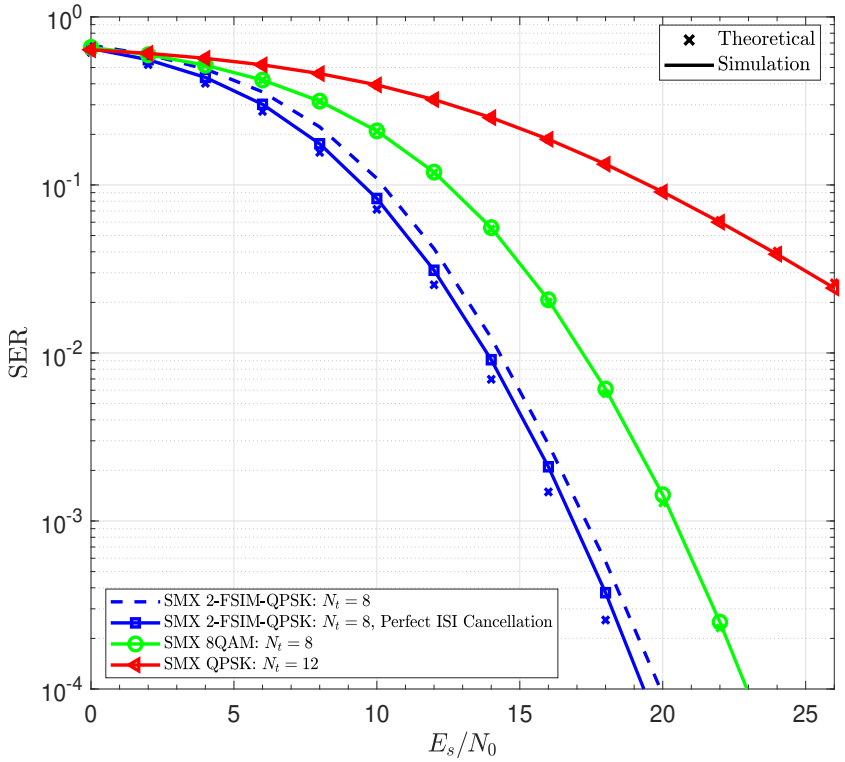

Figure 19: SER performance of the proposed SMX 2-FSIM-QPSK system and its equivalent SMX-QAM systems of same SE= 24 bpcu and $N_r = 12$.

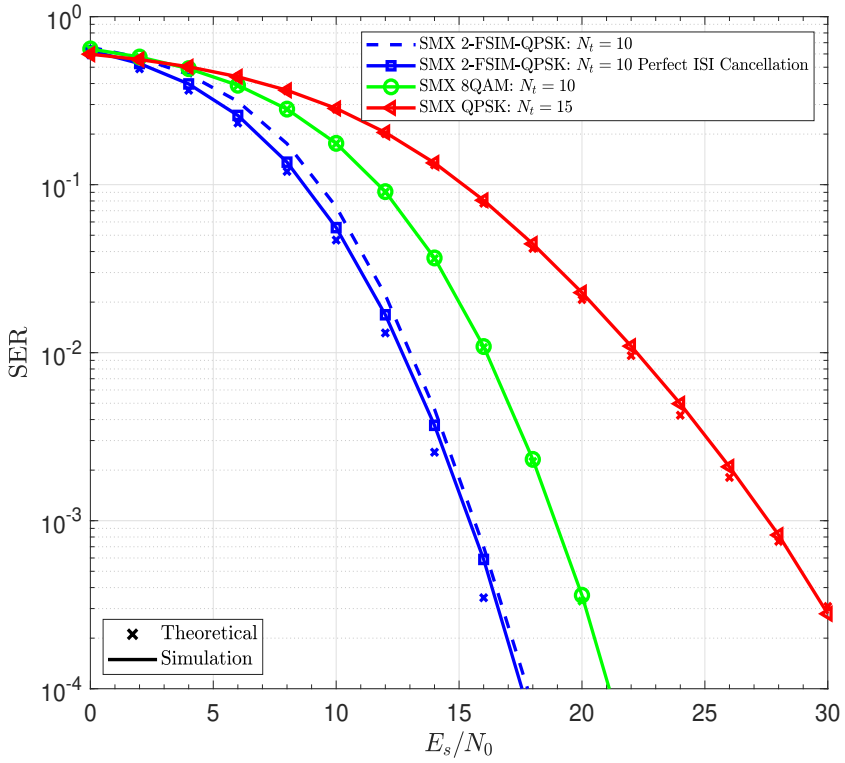

Figure 20: SER performance of the proposed SMX 2-FSIM-QPSK system and its equivalent SMX-QAM systems of same SE= 30 bpcu and $N_r = 16$.

Table 4: Spectral efficiency of different $N_t \times N_r$ MIMO systems.

	System Name	Spectral Efficiency $\mathcal{L}$ (bpcu)	N_a number of activated TA(s)
SMX	SMX-APM	$N_t \log_2 M$	N_t
	SMX-FSIM	$N_t \log_2 M + N_t \log_2 N$	N_t
Transmit Spatial IM	SSK[56]	$\lfloor \log_2 N_t \rfloor$	1
	GSSK[57]	$\lfloor \log_2 C_{N_t}^{N_a} \rfloor$	N_a
	Bi-SSK[54]	$2\lfloor \log_2 N_t \rfloor$	$N_a = 1$ for I/Q: $\{1, 2\}$
	ExSSK [58]	N_t	$\{0, \ldots, N_t\}$
	SM[59]	$\log_2 M + \lfloor \log_2 N_t \rfloor$	1
	GSM [60]	$N_a \log_2 M + \lfloor \log_2 C_{N_t}^{N_a} \rfloor$	N_a
	QSM[55]	$\log_2 M + 2\lfloor \log_2 N_t \rfloor$	$N_a = 1$ for I/Q: $\{1, 2\}$
	VGSM[61]	$\approx \log_2 M + \log_2(2^{N_t} - 1)$	$\{1, \ldots, N_t\}$

4.5 Spectral Efficiency Analysis: SMX-FSIM vs existing MIMO techniques

In this section, the SE of different MIMO techniques with different number of TAs N_t and modulation order M is analyzed. This comparison considers the conventional SMX with linear APM (QAM, PSK), and several transmit spatial modulations with/without APM that uses the TA(s) indices to convey additional information bits. The SE of these systems are summarized in Table 4 while assuming $N_r \geq N_t$, and Figs 21-22 compare their SEs as function of number of TAs with $M = 4$ and $M = 16$ respectively. For clarification, the Extended SSK (ExSSK) and Variable N_a GSM (VGSM) (shown in Table 4) allow a variable number of active TAs to increase the SE. For the same reason, a separate indexation for the in-phase and quadrature components is considered in Bi-SSK[54] and Quadrature SM [55].

Note that the SE of GSSK and GSM depends on the number of activated TAs N_a as shown in Table 4, and in these figures N_a is selected to achieve the maximum SE with a specific N_t that occurs when $N_a = \frac{N_t}{2}$ with GSSK (depends on M-ary order with GSM using $N_a < N_t$ to enable IM since GSM using $N_a = N_t$ is same as conventional SMX). Figs. 21-22 show that the transmit spatial IM schemes without APM (i.e. SSK [56], GSSK[57], Bi-SSK [54], ExSSK[58]) suffer from a limited SE gain, and thus they are more suitable for low data rates applications. Whereas a higher SE is reached when incorporating APM symbol transmission with IM (i.e., SM, GSM, QSM, etc.). It is clear that the highest SE is achieved by the conventional SMX-APM, GSM, and the proposed SMX-FSIM system due to the important multiplexing gain with/without IM. However, SMX-FSIM achieves 1.5 (resp. 1.25) times higher SE with 2 filters only compared to SMX-QPSK (resp. SMX-16QAM) as depicted in Fig. 21-22 where SMX-FSIM shows its superiority over all other MIMO techniques. In addition, it is worth mentioning that the number of activated TAs N_a with transmit spatial IM is less than N_t but they require full-RF transmit architecture (i.e. Number of RF chains =

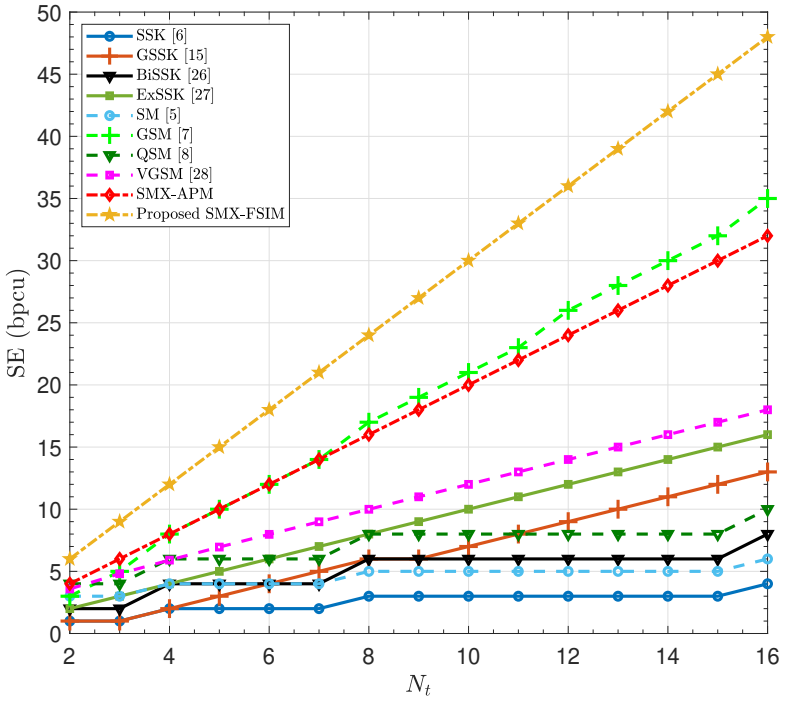

Figure 21: Maximum SE for different MIMO techniques: $M = 4$ for systems with APM, $N_a = [1, \ldots, N_t - 1]$ for fixed N_a schemes, and $N = 2$ for FSIM. Figure reproduced from [4].

N_t) to avoid SE degradation. Note that the transmit spatial IM schemes with RF-switching having the number of RF chains equals to the maximum N_a suffer from spectral regrowth due to pulse shaping time truncation to symbol period, and thus a SE degradation will occur [62]. Moreover, the RF-switching time at each symbol period introduces additional SE degradation [63]. Thus, the obvious solution for all transmit spatial IM is to use a full-RF transmit architecture to avoid this SE problem.

Performance results comparison of the SMX-FSIM, conventional SMX and GSM scheme in sub-THz environment, their computational complexity, PAPR and power consumption is detailed in [4] and deliverable D3.1 [5].

According to [4] and [5], SMX-FSIM requires less SNR to reach the desired performance even without channel coding, and the proposed system requires the minimum number of transmit antennas to achieve any SE, as shown in Figs. 21-22 that limit the transceiver cost and power consumption related to RF chains and to achieve the desired performance so a higher EE is provided. Hence, SMX-FSIM requires less parallel modulator and RF chains than the most spectral-efficient existing MIMO systems, which means lower hardware cost and power consumption even with PN impairment, as it is highlighted in [5]. This cost and power consumption of SMX-FSIM remains the minimum compared to the other candidates, even when considering a massive MIMO system exploiting beamforming gain to compensate the sub-THz/THz losses.

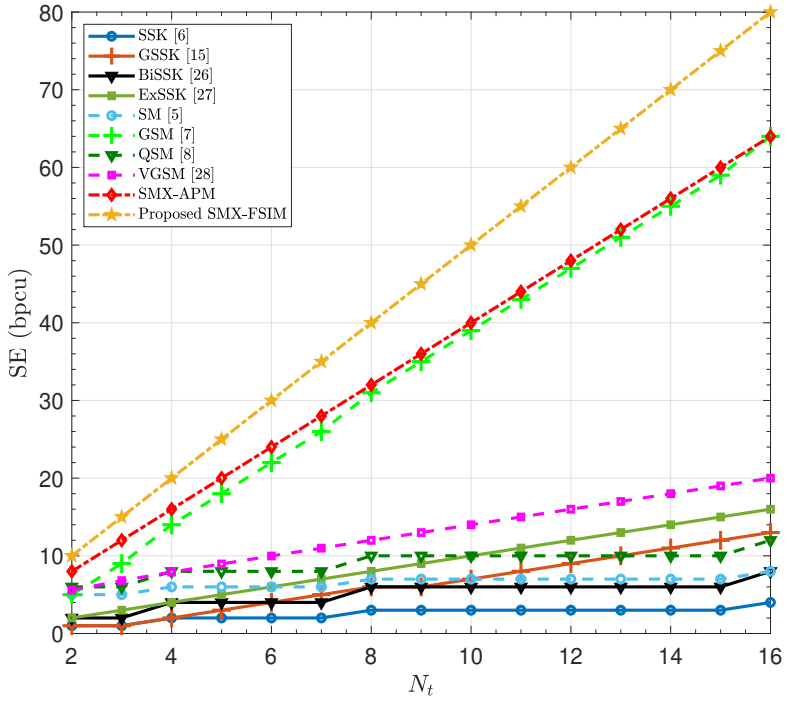

Figure 22: Maximum SE for different MIMO techniques: $M = 16$ for systems with APM, $N_a = [1, \ldots, N_t - 1]$ for fixed N_a schemes, and $N = 2$ for FSIM.Figure reproduced from [4].

4.6 Conclusion

The proposed SMX-FSIM system is shown to achieve the highest SE gain among the existing MIMO systems with/without IM even with 2 filter shapes and low order modulation. For instance, the achieved gain with SMX FSIM system is $N_t \log_2 N$ higher than that of SMX QAM using the same modulation order and the number of antennas. It is also important to mention that SMX FSIM fully utilizes all time, frequency, and spatial resources in contrast to spatial IM (e.g., GSM,...) that activates a certain number of antennas and requires a full-RF transmitter architecture. In the current study, we are focusing on an ultra-high data rates system for indoor scenarios with power and complexity constraints for the UE receiver, like downlink kiosk application and enhanced throughput WLAN. For this reason, we developed and theoretically assessed the proposed SMX FSIM system with a linear receiver based on ZF equalizer and parallel MF detectors that allow us to maintain a low and feasible receiver complexity. The performance of SMX-FSIM is very tight to the derived theoretical lower bound. Compared to the equivalent SMX QAM system of the same SE using either the same modulation order or the same number of TAs, the results reveal that SMX FSIM with a linear receiver and only two non-optimal filter shapes outperforms by 3.5 dB up to more than 12 dB these equivalent systems in Rayleigh channel. In order to complete our study and propose a new ultra-high data rate system in the sub-THz environment, a complete analysis in the sub-THz indoor environment with RF impairments is provided for the proposed system SMX FSIM, and the other candidates (SMX QAM and GSM) and detailed in [4] and [5]. Finally, we showed that SMX FSIM with a linear receiver has better performance and robustness to phase noise, lower transceiver cost, higher SE/EE gain, and lower power consumption

compared to its competitor candidates. Therefore, this analysis and discussion summarized in Table 5 promotes SMX-FSIM with a linear receiver as a very competitive candidate for low-power wireless ultra-high data rates system in sub-THz bands.

Table 5: Summary of different MIMO techniques for low-power wireless ultra-high data rates systems in sub-THz bands.

	MIMO systems with power-efficient low order APMs and linear based receivers		
Parameter	**SMX-FSIM**	**SMX-QAM**	**GSM** using full-RF Tx architecture
Spectral Efficiency (see Figs. 7-8)	$N_t(\log_2 M + \log_2 N)$ **High**	$N_t \log_2 M$ **Medium**	$N_a \log_2 M + \log_2 C_{N_t}^{N_a}$ where $N_a \leq N_t$ **Medium**
Robustness to PN (see Figs. 10-11)	**High**	**Low** to **Medium**	**Low** (**High** with ML[4])
PAPR (see Fig 12)	**Medium**	**Low**	**Low** to **High** (depend on M, N_a and N_t)
Energy Efficiency (see Table V)	**High**	**Medium**	**Medium**
Linear Detector Complexity (see Table IV)	**Medium** to **High** (depend on filter length)	**Medium**	**Low**
Cost based on number of RF chains (see sub-Section IV-C-3)	**Low**	**Low** to **Medium**	**High**
Flexibility (Reconfigurable System)	**High**	**Low**	**High**

5 Deliverable final conclusions

Results provided in this deliverable D2.1-addendum undertaken in WP2 constitute an extension to technical material in D2.1. First and very important result is the achievement of a novel dimension for indexation thanks to the development of the FSIM system, where a bank with different filter shapes is used. Note that this domain allows a SE enhancement by at least 1 bit/s/Hz in contrast to the existing domains in SISO (temporal and frequency domains) where their maximum enhancement is limited to 0.6 bit/s/Hz or less.

The theoretical lower bounds for filter error probability and BER are derived, and the analysis validates the achieved performance using the proposed FSIM approach. Monte Carlo simulations showed that the FSIM-QPSK system with 2 and 4 non-optimal filters offers, at BER= 10^{-4} and same SE, a gain of 3.8 dB and 1.7 dB as compared to their equivalent systems 8QAM and 16QAM, similarly, 4-FSIM-16QAM achieves a gain of 2.2 dB. Proposed FSIM scheme demonstrates that ISI is not necessarily undesirable while it is controllable and predictable, since it permits to achieve a higher system capacity compared to systems that enforce zero interference. Finally, it can be concluded that FSIM scheme can achieve even higher SE after designing a larger filter bank (higher N), and it is useful for ultra-high rate wireless communication.

Another big achievement is the development of generalized MIMO Spatial Multiplexing system, thanks to filter IM domain that generalizes many existing modulation and time/frequency IM domains. In particular, FSIM scheme is considered in the proposed system to achieve the highest SE gain (N_t log2 N) among the existing MIMO systems by conveying the additional bits in the index of the used filter shape at each transmitting antenna. The theoretical tight

lower bound of the proposed SMX FSIM system is derived and verified by Monte Carlo simulations. The proposed SMX 2-FSIM-QPSK achieves at least 3-4 dB gain compared to SMX 8QAM of the same SE and number of TAs, and the performance gain increases to more than 12 dB compared to SMX QPSK of the same SE and APM order.
The results from evaluations (different candidates for ultra-high data rates in sub-THz bands, e.g., SMX FSIM, SMX QAM, and GSM with linear receiver) reveals that SMX FSIM has better performance, higher robustness to PN, lower transceiver cost, higher SE/EE gain and less power consumption.
In order to complete our study and propose a new ultra-high data rate system in the sub-THz environment, a complete analysis in the sub-THz indoor environment with RF impairments is provided for the proposed system SMX FSIM, and the other candidates (SMX QAM and GSM) (more details are presented in [4] and [5]). Finally, we showed that SMX FSIM with a linear receiver has better performance and robustness to phase noise, lower transceiver cost, higher SE/EE gain, and lower power consumption compared to its competitor candidates. However, these advantages comes with a slight receiver complexity increase which is in order of L times higher than other candidates, and this complexity can be reduced by proper design of filter bank with shorter filter length L while respecting FSIM scheme filter requirements. Finally, it is worth mentioning that SMX FSIM in sub-THz channel requires much lower SNR which is crucial for sub-THz systems with limited output power as highlighted in [5], and it is the only scheme among these candidates that can operates in a medium PN level with linear low complexity receiver. Therefore, this analysis and discussion summarized in Table 5 promotes SMX-FSIM as a very competitive candidate for low-power wireless ultra-high data rates system in sub-THz bands.

Finally, the current and future works include many possible enhancements for the proposed system by considering the optimal filter bank design to maximize the SE/EE gains and minimize the system cost. In addition, FSIM based concept is also extended to achieve much higher SE gain, and its coded version is considered to reach the target performance at very low SNR and transmit output power.

References

[1] M. Saad, N. Bouhlel, F. Bader, S. Bicaïs, J-B Doré, Y. Corre, M. Z. Aslam, "Propagation channel model and RF impairments definition and waveform design," French funded project-ANR-17-CE25-0013 BRAVE, Tech. deliverable BRAVE D2.1, Nov. 2020.

[2] M. Saad, A. C. Al Ghouwayel, H. Hijazi, F. Bader, and J. Palicot, "MIMO techniques for wireless Terabits systems under sub-THz channel with RF impairments," in 2020 IEEE International Conference on Communications Workshops, Dublin, Ireland, Jun. 2020, pp. 1-6.

[3] M. Saad, J. Palicot, F. Bader, A. C. Al Ghouwayel, and H. Hijazi, "A Novel Index Modulation Dimension based on Filter Domain: Filter Shapes Index Modulation," at the IEEE Transactions on Communications, Nov. 2020, doi: 10.1109/TCOMM.2020.3039842.

[4] M. Saad, N. Al Akkad, H. Hijazi, A. C. Al Ghouwayel, F. Bader and J. Palicot, "Novel MIMO Technique for Wireless Terabits Systems in Sub-THz Band," in IEEE Open Journal of Vehicular Technology, vol. 2, pp. 125-139, 2021.

[5] J-B Doré, M. Alawieh, Y. Corre, M. Saad, F. Bader, "Performance assessments," French funded project-ANR-17-CE25-0013 BRAVE, Tech. deliverable BRAVE D3.1, Oct. 2021.

[6] R. Y. Mesleh, H. Haas, S. Sinanovic, C. W. Ahn and S. Yun, "Spatial modulation," *IEEE Trans. Veh. Technol.*, vol. 57, no. 4, pp. 2228-2241, July 2008.

[7] A. Younis, N. Serafimovski, R. Mesleh, and H. Haas, "Generalised spatial modulation," in Proc. Signals, Syst. Comput., pp. 1498- 1502, 2010.

[8] J. T. Wang, S. Y. Jia, J. Song, "Generalised spatial modulation system with multiple active transmit antennas and low complexity detection scheme," *IEEE Trans. Wireless Commun.*, vol.11, no. 4, pp. 1605-1615, Apr. 2012.

[9] P. Liu, M. Di Renzo and A. Springer, "Variable- N_u generalized spatial modulation for indoor LOS mmWave communication: Performance optimization and novel switching structure," *IEEE Trans. Commun.*, vol. 65, no. 6, pp. 2625-2640, June 2017.

[10] E. Basar, U. Aygolu, E. Panayirci, and H. V. Poor, "Orthogonal frequency division multiplexing with index modulation," *IEEE Trans. Signal Process.*, vol. 61, no. 22, pp. 5536-5549, 2013.

[11] D. Tsonev, S. Sinanovic, and H. Haas, "Enhanced subcarrier index modulation (SIM) OFDM," in Proc. IEEE GLOBECOM Workshops, Dec. 2011, pp. 728-732.

[12] E. Öztürk, E. Basar and H. A. Çırpan, "Generalized frequency division multiplexing with flexible index modulation numerology," *IEEE Signal Process. Lett.*, vol. 25, no. 10, pp. 1480-1484, Oct. 2018.

[13] M. Nakao, T. Ishihara, and S. Sugiura, "Single-carrier frequency domain equalization with index modulation," *IEEE Commun. Lett.*, vol. 21, no. 2, pp. 298-301, Feb. 2017.

[14] M. Chafii, F. Bader and J. Palicot, "SC-FDMA with index modulation for M2M and IoT uplink applications," in 2018 IEEE Wireless Commun. and Netw. Conf. (WCNC), Barcelona, 2018, pp. 1-5.

[15] E. Başar, "Multiple-input multiple-output OFDM with index modulation," *IEEE Signal Process. Lett.*, vol. 22, no. 12, pp. 2259-2263, Dec. 2015.

[16] H. A. Ngo, C. Xu, S. Sugiura and L. Hanzo, "Space-time-frequency shift keying for dispersive channels," *IEEE Signal Process. Lett.*, vol. 18, no. 3, pp. 177-180, Mar. 2011.

[17] French funded project-ANR-17-CE25-0013, "Back to single-carrier for beyond-5G communications above 90 GHz-(BRAVE)," [Online]. Available: http://www.brave-beyond5g.com/.

[18] Y. Corre, G. Gougeon, J.-B. Doré, S. Bicaïs, B. Miscopein, E. Faussurier, M. Saad, J. Palicot, and F. Bader, "Sub-THz spectrum as enabler for 6G wireless communications up to 1 Tbit/s," in 6G Wireless Summit, Levi Lapland, Finland, Mar. 2019.

[19] M. Saad, F. Bader, J. Palicot, Y. Corre, G. Gougeon, J-B Doré, "Beyond-5G wireless Tbps scenarios and requirements," French funded project-ANR-17-CE25-0013 BRAVE, Tech. Report BRAVE D1.0, 2018. [Online]. Available: https://hal.archives-ouvertes.fr/hal-01947363/document.

[20] M. Saad, F. Bader, J. Palicot, A. C. Al Ghouwayel, and H. Hijazi, "Single carrier with index modulation for low power terabit systems," in 2019 IEEE Wireless Communications and Networking Conference (WCNC), Marrakech, Morocco, Apr. 2019, pp. 1–7.

[21] M. Saad, F. C. Lteif, A. C. Al Ghouwayel, H. Hijazi, J. Palicot, and F. Bader, "Generalized spatial modulation in highly correlated channels," in 2019 IEEE 30th International Symposium on Personal, Indoor and Mobile Radio Communications (PIMRC Workshops), Istanbul,Turkey, Sep. 2019, pp. 1-6.

[22] M. Saad, F. Bader, A. C. Al Ghouwayel, H. Hijazi, N. Bouhel, and J. Palicot, "Generalized spatial modulation for wireless Terabits systems under sub-THz channel with RF impairments,"in ICASSP 2020 -2020 IEEE International Conference on Acoustics, Speech and Signal Processing (ICASSP), Barcelona, Spain, May 2020, pp. 5135-5139.

[23] J. Pierce, "Optical channels: Practical limits with photon counting," *IEEE Trans. Commun.*, vol. COM-26, no. 12, pp. 1819-1821, Dec. 1978.

[24] X. Liu, T. H. Wood, R. W. Tkach and S. Chandrasekhar, "Demonstration of record sensitivity in an optically pre-amplified receiver by combining PDM-QPSK and 16-PPM with pilot-assisted digital coherent detection," *Optical Fiber Commun. Conf. and Exposition and the National Fiber Optic Engineers Conf.*, Los Angeles, CA, 2011, pp. 1-3.

[25] G. Cheng, L. Wang, W. Xu and G. Chen, "Carrier index differential chaos shift keying modulation," in *IEEE Trans. Circuits and Systems II: Express Briefs*, vol. 64, no. 8, pp. 907-911, Aug. 2017.

[26] G. Kaddoum, Y. Nijsure and H. Tran, "Generalized code index modulation technique for high-data-rate communication systems," in *IEEE Trans. Veh. Technol.*, vol. 65, no. 9, pp. 7000-7009, Sept. 2016.

[27] A. M. Jaradat, J. M. Hamamreh and H. Arslan, "OFDM with subcarrier number modulation," *IEEE Wireless Commun. Lett.*, vol. 7, no. 6, pp. 914-917, Dec. 2018.

[28] S. Dang, G. Ma, B. Shihada and M. Alouini, "Enhanced orthogonal frequency-division multiplexing with subcarrier number modulation," *IEEE Internet of Things Journal*, vol. 6, no. 5, pp. 7907-7920, Oct. 2019.

[29] S. Althunibat, R. Mesleh and T. F. Rahman, "A novel uplink multiple access technique based on index-modulation concept," *IEEE Trans. Commun.*, vol. 67, no. 7, pp. 4848-4855, July 2019.

[30] S. Althunibat, R. Mesleh and K. Qaraqe, "Quadrature Index Modulation Based Multiple Access Scheme for 5G and Beyond," in *IEEE Commun. Lett.*, vol. 23, no. 12, pp. 2257-2261, Dec. 2019.

[31] S. Althunibat, R. Mesleh and K. A. Qaraqe, "IM-OFDMA: A Novel Spectral Efficient Uplink Multiple Access Based on Index Modulation," in *IEEE Trans. Veh. Technol.*, vol. 68, no. 10, pp. 10315-10319, Oct. 2019.

[32] R. Fan, Y. J. Yu and Y. L. Guan, "Generalization of orthogonal frequency division multiplexing with index modulation," *IEEE Trans. Wireless Commun.*, vol. 14, no. 10, pp. 5350-5359, Oct. 2015.

[33] M. Wen, B. Ye, E. Basar, Q. Li and F. Ji, "Enhanced orthogonal frequency division multiplexing with index modulation," *IEEE Trans. Wireless Commun.*, vol. 16, no. 7, pp. 4786-4801, July 2017.

[34] T. Ishihara and S. Sugiura, "Faster-than-nyquist signaling with index modulation," *IEEE Wireless Commun. Lett.*, vol. 6, no. 5, pp. 630-633, Oct. 2017.

[35] M. Nakao and S. Sugiura, "Spectrally efficient frequency division multiplexing with index-modulated non-orthogonal subcarriers," *IEEE Wireless Commun. Lett.*, vol. 8, no. 1, pp. 233-236, Feb. 2019.

[36] M. Nakao, T. Ishihara and S. Sugiura, "Dual-mode time-domain index modulation for nyquist-criterion and faster-than-nyquist single-carrier transmissions," *IEEE Access*, vol. 5, pp. 27659-27667, 2017.

[37] M. Nakao and S. Sugiura, "Dual-mode time-domain single-carrier index modulation with frequency-domain equalization," in 2017 IEEE 86th Veh. Technol. Conf. (VTC-Fall), Toronto, Ontario, 2017, pp. 1-5.

[38] T. Mao, Z. Wang, Q. Wang, S. Chen and L. Hanzo, "Dual-mode index modulation aided OFDM," *IEEE Access*, vol. 5, pp. 50-60, 2017.

[39] T. Mao, Q. Wang and Z. Wang, "Generalized dual-mode index modulation aided OFDM," *IEEE Commun. Lett.*, vol. 21, no. 4, pp. 761-764, Apr. 2017.

[40] M. Wen, E. Basar, Q. Li, B. Zheng and M. Zhang, "Multiple-Mode Orthogonal Frequency Division Multiplexing With Index Modulation," in *IEEE Trans. Commun.*, vol. 65, no. 9, pp. 3892-3906, Sept. 2017.

[41] M. Wen, Q. Li, E. Basar and W. Zhang, "Generalized Multiple-Mode OFDM With Index Modulation," in *IEEE Trans. Wireless Commun.*, vol. 17, no. 10, pp. 6531-6543, Oct. 2018.

[42] J. Li, S. Dang, M. Wen, X. Jiang, Y. Peng and H. Hai, "Layered Orthogonal Frequency Division Multiplexing With Index Modulation," in *IEEE Systems Journal*, vol. 13, no. 4, pp. 3793-3802, Dec. 2019.

[43] T. Mao, Q. Wang, Z. Wang and S. Chen, "Novel Index Modulation Techniques: A Survey," in *IEEE Commun. Surveys & Tutorials*, vol. 21, no. 1, pp. 315-348, Firstquarter 2019.

[44] F. Pancaldi, G. M. Vitetta, R. Kalbasi, N. Al-Dhahir, M. Uysal and H. Mheidat, "Single-carrier frequency domain equalization," in IEEE Signal Process. Mag., vol. 25, no. 5, pp. 37-56, September 2008.

[45] J. Proakis and M. Salehi, *Digital communications*. Boston, MA: McGraw-Hill, 2008.

[46] K. Berberidis and P. Karaivazoglou, "A block adaptive DFE in the frequency domain based on tentative decisions," in 9th Eur. Signal Process. Conf. (EUSIPCO 1998), Rhodes, 1998, pp. 1-4.

[47] E. Seifi, M. Atamanesh, and A. K. Khandani, "Media-based MIMO: A new frontier in wireless communication," Oct. 2015. [Online]. Available: arxiv.org/abs/1507.07516

[48] E. Basar, "Media-Based Modulation for Future Wireless Systems: A Tutorial," IEEE Wireless Communications, vol. 26, no. 5, pp. 160–166, Oct. 2019.

[49] A. Mokh, M. Helard and M. Crussiere, "Space Shift Keying Modulations for Low Complexity Internet-of-Things Devices," GLOBECOM 2017 - IEEE Global Commun. Conf., Singapore, 2017, pp. 1-7.

[50] S. Bicais and J.-B. Doré, "Phase noise model selection for sub-THz communications,"in 2019 IEEE Global Communications Conference (GLOBECOM), Waikoloa, HI, USA, Dec. 2019, pp. 1-6.

[51] M. R. Khanzadi, D. Kuylenstierna, A. Panahi, T. Eriksson, and H. Zi-rath, "Calculation of the performance of communication systems from measured oscillator phase noise," IEEE Transactions on Circuits and Systems I: Regular Papers, vol. 61, no. 5, pp. 1553-1565, May 2014.

[52] G. Gougeon, Y. Corre, and M. Z. Aslam, "Ray-based deterministic channel modelling for sub-THz band," in 2019 IEEE 30th International Symposium on Personal, Indoor and Mobile Radio Communications (PIMRC Workshops), Istanbul, Turkey, Sep. 2019, pp. 1–6.

[53] J. Xu, X. Tao, and P. Zhang, "Analytical SER performance bound of M-QAM MIMO system with ZF-SIC receiver," in 2008 IEEE International Conference on Communications, Beijing, China, 2008, pp. 5103–5107.

[54] H.-W. Liang, R. Y. Chang, W.-H. Chung, H. Zhang, and S.-Y. Kuo, "Bi-space shift keying modulation for MIMO systems," IEEE Communications Letters, vol. 16, no. 8, pp. 1161–1164, Aug. 2012.

[55] R. Mesleh, S. S. Ikki, and H. M. Aggoune, "Quadrature spatial modulation," IEEE Transactions on Vehicular Technology, vol. 64, no. 6, pp. 2738-2742, Jun. 2015.

[56] J. Jeganathan, A. Ghrayeb, L. Szczecinski, and A. Ceron, "Space shift keying modulation for MIMO channels," at IEEE Transactions on Wireless Communications, vol. 8, no. 7, pp. 3692-3703, Jul. 2009.

[57] J. Jeganathan, A. Ghrayeb, and L. Szczecinski, "Generalized space shift keying modulation for MIMO channels,"in 2008 IEEE 19th International Symposium on Personal, Indoor and Mobile Radio Com-munications, Cannes, France, Sep. 2008, pp. 1-5.

[58] A. Mokh, M. Helard, and M. Crussiere, "Space Shift Keying Modulations for Low Complexity Internet-of-Things Devices," in GLOBECOM 2017 - 2017 IEEE Global Communications Conference, Singapore, Dec. 2017, pp. 1–7.

[59] R. Y. Mesleh, H. Haas, S. Sinanovic, C. W. Ahn, and S. Yun, "Spatial modulation," at IEEE Transactions on Vehicular Technology, vol. 57, no. 4, pp. 2228-2241, Jul. 2008.

[60] J. T. Wang, S. Y. Jia, and J. Song, "Generalised spatial modulation system with multiple active transmit antennas and low complexity detection scheme," a IEEE Transactions on Wireless Communications, vol. 11, no. 4, pp. 1605-1615, Apr. 2012.

[61] P. Liu, M. Di Renzo, and A. Springer, "Variable- Nu generalized spatial modulation for indoor LOS mmWave communication: Performance optimization and novel switching structure," IEEE Transactions on Communications, vol. 65, no. 6, pp. 2625–2640, Jun. 2017.

[62] K. Ishibashi and S. Sugiura, "Effects of antenna switching on band-limited spatial modulation," IEEE Wireless Communications Letters, vol. 3, no. 4, pp. 345–348, Aug. 2014.

[63] E. Soujeri and G. Kaddoum, "The impact of antenna switching time on spatial modulation," IEEE Wireless Communications Letters, vol. 5, no. 3, pp. 256–259, Jun. 2016.